Statistical properties of incompressible passive vector convected by isotropic turbulence

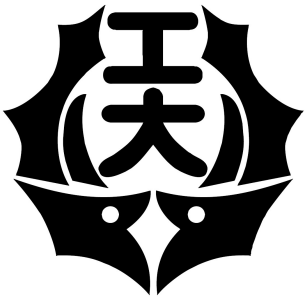

Yang Jingyuan

Department of Scientific and Engineering Simulation

Nagoya Institute of Technology

A thesis submitted for the degree of

Doctor of Engineering

March, 2020

Abstract

This paper investigates statistical properties of an incompressible passive vector convected by homogeneous isotropic turbulence by comparing to the velocity and passive scalar, in order to explore the physics behind the differences and similarities in the statistical properties between the velocity vector and passive scalar. The passive vector obeys an equation similar to the Navier-Stokes equation which has a pseudopressure term to ensure the incompressibity and the pseudoviscosity but the convective term is linear. Direct numerical simulations (DNSs) with resolution of 1024^3 grid points were performed with Reynolds numbers $R_\lambda \sim 90$, 200, 300 and 400. Visualizations show that the geometry of pseudoenstropy is sheetlike, similar to a passive scalar, but different to the velocity field which has tubelike structures. The pseudoenergy spectrum obeys the $k^{-5/3}$ power law, similar to the kinetic enegy spectrum, and the Kolmogorov Constants are found to be $C_K = 1.57$ for the velocity, $C_{PV} = 1.0$ for the passive vector, and $C_{OC} = 0.67$ for the passive scalar, respectively. The 4/3 law for the cubic moment which is the average of the production of the longitudinal velocity increment and the square of the passive vector increment is analytically derived from the equation of the passive vector and confirmed by the DNS. The one point probability density function (PDF) of the passive vector is wider than that of velocity which is closer to a Gaussian distribution. The right tail of the PDFs of the logarithm of the dissipation rates of the kinetic energy and pseudoenergy are similar, and well approximated by a log-normal distribution. The left tailf of PDF of the the dissipation rate obey power laws which consist with the prediction based on chi-square distribution. The PDF of pressure is negatively skewed, whereas the

pseudopressure PDF is nearly symmetric. The scaling exponents of the passive vector are anomalous, non-universal for high orders, and have values between that of velocity and the passive scalar for orders greater than 4. It is suggested that 1) the small scale statistical properties of the passive vector are more similar to those of the passive scalar than those of velocity; 2)the nonlinearity of the Navier-Stokes equation leads anomalous but universal scaling exponents, and the linearity of the equations of the passive fields bears nonuniversal scaling exponents and stronger intermittency than the velocity.

To my loving parents,

without your supports, I wouldn't begin my studies at graduated school and finish my academic career at Nagoya Institute of Technology.

Contents

List of Figures

LIST OF FIGURES

List of Tables

LIST OF TABLES

1

Introduction

1.1 Brief History of Turbulence Research

Turbulence is ubiquitous, occurring in the atmosphere and ocean, in winds and rivers, inside combustion engines, airplanes and power plants, and, in daily life, in hot water in kettles and the bath tub. Velocity and pressure in turbulent flow fluctuate strongly in space and time, but accurate prediction of these variables is almost impossible; thus, as an alternative, its statistical law has been studied since Reynolds' pioneering work.[1] One important property of turbulence is its huge ability to transport heat and mass, which is widely exploited within industry and daily life. Therefore, it is very important to understand, predict, and control the turbulent flow that transfers and mixes heat and mass. However, there is still a lack of understanding of turbulent flow in spite of longstanding efforts, due to strong nonliearity, infinite degrees of freedom, and dissipative nature of the Navier-Stokes equation.

Kolmogorov[2] made great progress toward understanding turbulence, deriving a statistical law of velocity fluctuations at small scales with the two hypothesis and the dimensional arguments. When the Reynolds number is very large, there exists the inertial range $\eta \ll r \ll L$ in which the nonlinearity is dominant in the dynamics and neither large scale properties of the flow nor the viscosity are relevant (See details in Section 2.5), where L is defined as a macro-length scale for turbulence, and η is the dissipation scale, known as the Kolmogorov length. In

the inertial range the moments of the velocity increments $\delta_r u(r) = u(x+r) - u(x)$ at separation distance r of two points obey the power law

$$\langle [\delta_r u(r)]^p \rangle = A_p (\bar{\epsilon} r)^{\xi_p}, \qquad \xi_p = \frac{p}{3}, \tag{1.1}$$

where $\langle\ \rangle$ means ensemble averaging, $\bar{\epsilon}$ is the mean kinetic energy dissipation rate per unit mass and A_p is non-dimensional constant which is not detemined within his theory except A_3. Kolmogorov derived analytically the third order moment as

$$\left\langle [\delta_r u(r)]^3 \right\rangle = -\frac{4}{5} \bar{\epsilon} r, \tag{1.2}$$

now known as Kolmogorov's 4/5 law which is the only asymptotically exact result known of in the context of turbulence. The Fourier transform of $\left\langle [\delta_r u(r)]^2 \right\rangle$ gives the kinetic energy spectrum, known as the Kolmogorov spectrum,

$$E(k) = C_K \bar{\epsilon}^{2/3} k^{-5/3}, \tag{1.3}$$

where C_K is the Kolmogorov constant. Many experiments and recent high-resolution simulations have shown that that Kolmogorov spectrum is observed regardless of flow type when the Reynolds number is large enough (see Fig. 1.1).

Most striking feature of the Kolmogorv theory is the prediction of existence of an universal statistical law irrespective of types of turbulent flow. The idea of universality has been much influenced from the success of the statistical mechanics for the phase transition. The scaling exponent $\xi_p = p/3$ of Eq.(1) is a linear function of order p, which represents the normal scaling. However, many studies have found that scaling exponents are not linear in p, instead increasing gradually with the order due to anomalous scaling (see Fig. 1.2). Anomalous scaling exponents are considered to closely relate to the occurrence of extreme turbulence events, also known as intermittency. This raises questions as to investigate whether the scaling exponents for turbulence are universal, and how we compute them using fundamental equations. Present understanding remains limited, and answering the above questions is an important issue in turbulence research.

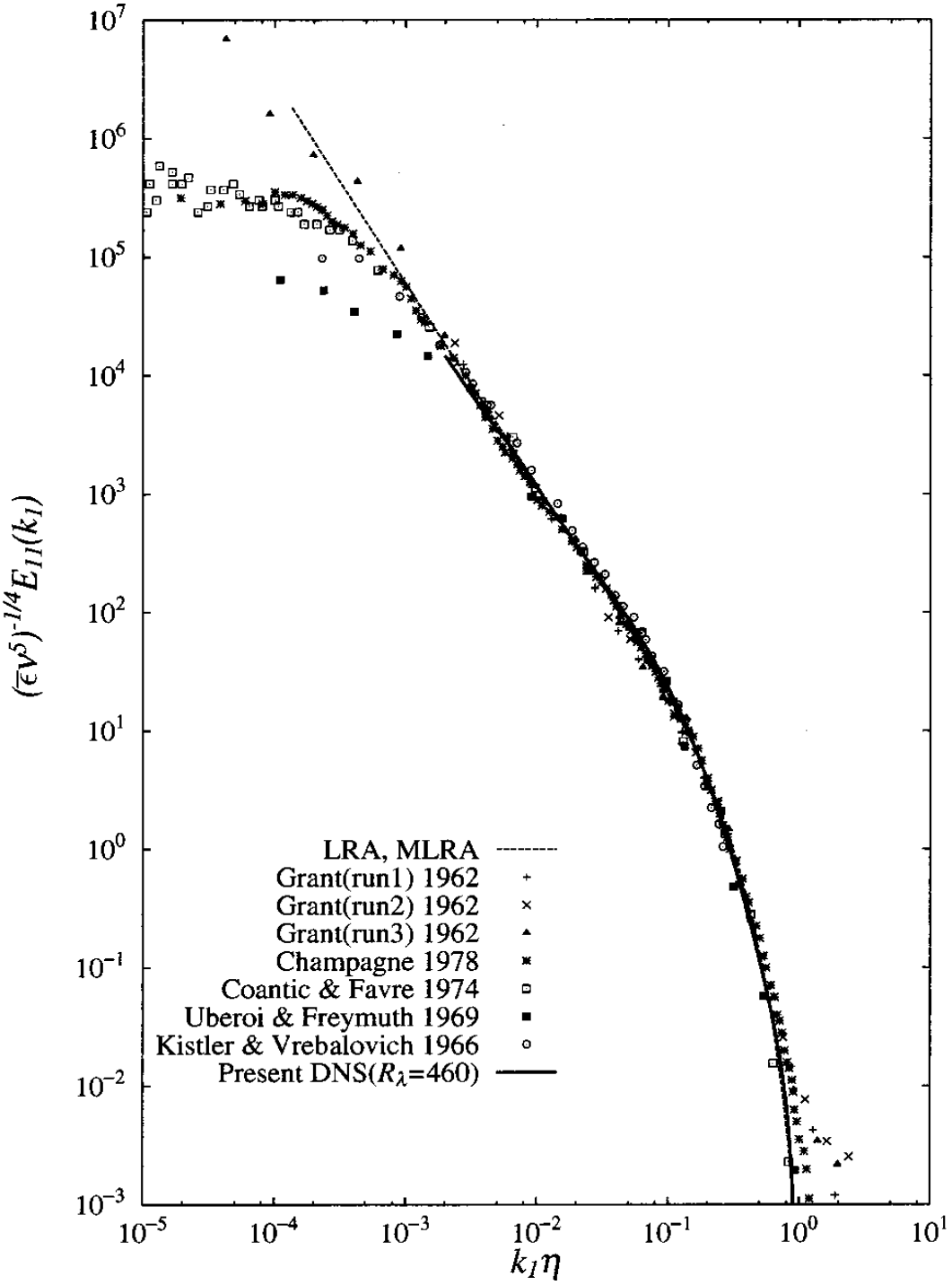

Figure 1.1: One dimensional spectra of kinetic energy.[3] Symbols denote results from experiments, solid lines for results from DNS, dotted line for results from LRA(Lagrangian renormalized approximation, one of the turbulent models).

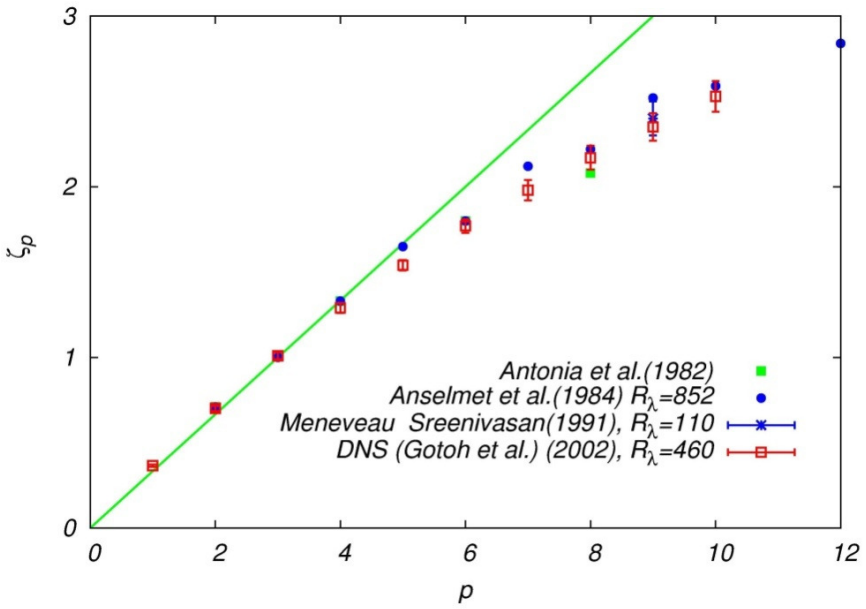

Figure 1.2: Scaling exponents of moment of longitudinal velocity increment. One can find that when $p > 3$, ξ_p^{uL} is smaller than $p/3$ by the Kolmogorov theory.

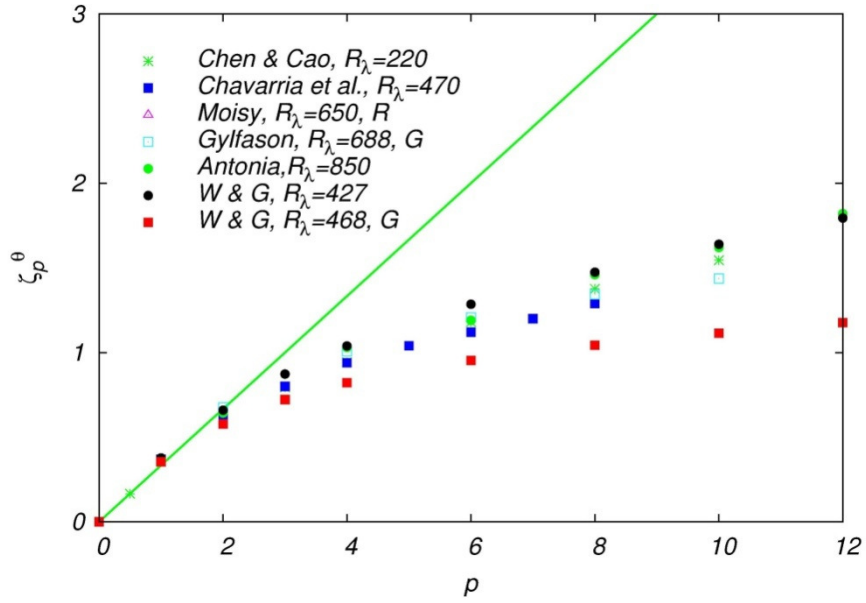

Figure 1.3: Scaling exponents of moment of longitudinal velocity increment. One can find that when $p > 3$, ξ_p^θ scatter more than ξ_p^{uL}, i.e. more magnitude small than $p/3$.

1.2 Passive Scalar in Turbulence

Heat and mass are transferred and mixed via fluid motion, which can transport aerosols, water vapor, chemical pollutants, and cloud droplets. In engineering and other real-life scenarios, substantial quantities of scalars can be transferred. Fuel and oxygen should be mixed as much as possible in combustion engines to maximize efficiency, while boilers are designed to avoid heat loss. Prediction of the dispersion of air pollutants, such as radioactive substances and pollen, is becoming more important in the context of the environment. It is essential to understand the mixing and transfer of scalars by turbulence. When the influence of a scalar on fluid motions is small, such as negligible buoyancy force in thermal convections, the scalar is referred to as passive. In addition to turbulence itself, the mixing of passive scalars is a canonical problem in the fundamental physics of turbulence.[4,5] The governing equation of a passive scalar $\theta(\boldsymbol{x}, t)$ is similar to the Navier-Stokes equation, where convection is due to turbulent velocity and dissipation (smearing) to molecular diffusivity, but lacks a pressure term:

$$(\frac{\partial}{\partial t} + \boldsymbol{u} \cdot \nabla)\theta = \kappa \nabla^2 \theta + f^\theta, \tag{1.4}$$

where κ denotes the diffusive coeffient normalized by density, f^θ denotes the external scalar fluctuation injection which plays a role like the external forcing to velocity. These properties simplify the equation, linear, local in space and applicable to a single component; in contrast, the Navier-Stokes equation usually applies to all three components, is nonlinear and nonlocal in space, and the velocity vector can be solenoidal. Thus, it is reasonable to assume that mathematical and physical analysis of the statistical properties of scalar fluctuations is simpler than that of the turbulent velocity field. Passive scalars have similar statistical properties to velocity fluctuations, e.g., the existence of an inertial convective range: $\max(\eta, \eta_\theta) \ll r \ll \min(L, L_\theta)$, where L_θ denotes the integral (or forcing) scale of a passive scalar, and $\eta_\theta = \eta(\kappa/\nu)^{1/2}$ denotes the diffusive scale of a passive scalar. In the inertial convective range; following Kolmogorov,[2] the spectrum of the passive scalar variance is given as

$$E_\theta(k) = C_{OC} \bar{\epsilon}^{-1/3} \bar{\epsilon}_\theta k^{-5/3}, \tag{1.5}$$

where C_{OC} is the Obukhov-Corrsin constant, and $\bar{\epsilon}_\theta$ is the mean destruction rate of a scalar per unit mass (hereafter, the scalar dissipation rate). Yaglom's 4/3 law for structure function

$$-\frac{3}{4}\bar{\epsilon}_\theta = \left\langle \delta_r u_L (\delta_r \theta)^2 \right\rangle , \tag{1.6}$$

and the power law for the moments of the scalar increment

$$\langle (\delta_r \theta)^p \rangle \propto r^{\xi_p^\theta}, \qquad \xi_p^\theta = \frac{p}{3} \tag{1.7}$$

were developed.[6,7,8,7,9,10,11]

Although the statistics of scalars at low order moments are similar to those of velocity, it is widely recognized that in the inertial convective range, the scaling exponents of the moments of a passive scalar at high order are smaller than those of velocity. They also tend to saturate (Fig. 1.3), meaning that a passive scalar is more intermittent than the velocity field,[12,13,14,15,16,17] and also that the spatial structure of large scalar gradients is sheetlike, in contrast to the vortex tubes observed for velocity.[15,18,19,20]

Kraichnan[11,21] proposed a model for passive scalars, in which the velocity field is assumed to follow a Gaussian distribution with a delta correlation in time (known as the Kraichnan velocity ensemble). The most distinctive aspect of the model is that the scaling exponents of the scalar increments are derived analytically. They are determined by the zero mode (i.e., homogeneous solution) of the linear operator for the scalar moments, and are thus universal.[22] The model has also been extended to many other problems, such as the passive magnetic field,[23] passive scalars in the inverse cascade range for incompressible[13,24] and compressible[25] Kraichnan velocity ensembles, and finitely correlated Gaussian velocity ensembles.[26] It is held that when the velocity field is (nearly) Gaussian, the analyses in terms of the zero mode of the linear operator are applicable, as is the universality of the scaling components for the passive scalar moments. However, the turbulent velocity field in three dimensions, obeying the Navier-Stokes equation, differs significantly to the Kraichnan velocity ensemble, being neither Gaussian nor white noise, and the energy is forward-cascading. For example, Gotoh and Watanabe[27] studied the intermittency of two passive scalars convected by the same three-dimensional turbulent velocity field and governed by

the Navier-Stokes equation, but excited by different mechanisms (one being the uniform mean gradient and the other being Gaussian random injection, that is, white noise in time). It has been found that the scaling exponents of the moments of scalar increments differ at large scales and are therefore not universal. The above statistical law, in addition to various data from experiments and numerical simulations, suggest that passive scalar fluctuations are not as universal as for velocity, and that our understanding of the universality of passive scalar fluctuations is still lacking. Therefore, it is important to explore the physics responsible for the differences in statistical properties between velocity and passive scalars, such as scaling exponents and probability density functions (PDFs). To do this, it is helpful and effective to introduce an equation for a passive vector, which shares common properties with the Navier-Stokes and passive scalar equations. The statistical properties of the passive vector can then be compared with those of velocity and passive scalars.

Previously, Yoshida and Kaneda[28] studied the anomalous scaling of the anisotropy of second-order moments of a passive vector for the Kraichnan velocity ensemble in two dimensions. A passive vector $\boldsymbol{w}$ is defined as follows:

$$\left(\frac{\partial}{\partial t} + \boldsymbol{u}\cdot\nabla\right)\boldsymbol{w} = -\nabla q + \gamma\boldsymbol{w}\cdot\nabla\boldsymbol{u} + \alpha\nabla^2\boldsymbol{w}, \tag{1.8}$$

$$\nabla\cdot\boldsymbol{w} = 0, \tag{1.9}$$

where γ is a non-dimensional constant. When $\gamma = 1$, the pressure term can be eliminated, and Eq. (1.9) describes a passive magnetic field "$\boldsymbol{w}$", excited by the following term: $\gamma\boldsymbol{w}\cdot\nabla\boldsymbol{u}$. When $\gamma = -1$, Eq. (1.9) becomes linear with small disturbances $\boldsymbol{w}$ to the basic flow $\boldsymbol{u}$, and is excited by basic flow. When $\gamma = 0$, Eq. (1.9) describes a velocity-like convected field, which is the main objective of this study. Yoshida and Kaneda showed analytically that the exponent of the isotropic sector of the structure functions is independent of the existence of a pressure-like term, while the anisotropic sector depends upon the presence of a pressure-like term. Adzhemyan[29] studied cases with arbitrary γ (where γ is a real number) for the Kraichnan velocity ensemble in $\mathcal{D}$ dimensions using renormalization group (RG) analysis, and found that when $\gamma = 0$, normal scaling is present. Ohkitani[30] used direct numerical simulation (DNS) to investigate passive magnetic vectors,

the effects of the Biat-Savart law, and the depletion of nonlinearity, and found that a passive magnetic field tends to be more stretched than velocity over short time scales. Benzi, Biferale and Toschi[31] studied scaling exponents of the moments of increments and fluxes of passive vectors using a shell model, and found they are the same as the velocity field. Ching et al.[32] carried out simulations using shell models for passive and active vectors, and found that the scaling exponents of a convected field are dominated by zero modes, regardless of whether or not they are active. Using RG theory, Antonov et al.[33,34,35] studied the anomalous scaling of solenoidal passive vectors convected by a Gaussian random velocity with a finite correlation time. They investigated the universality of the scaling exponents, and their dependence on forcing, large-scale anisotropy, compressibility, and pressure.

We emphasize that our goal and starting point are to investigate the physics arising from the subtly distinctive properties of the velocity field and passive scalars. In this study, the equation for a passive vector should share the structure, and many other properties, of both the Navier-Stokes and passive scalar equations. Moreover, knowing that the Kraichnan velocity ensemble modified the properties of passive scalars, we choose DNS for our simulations, where the velocity field is directly governed by the Navier-Stokes equation. Passive vectors in this study are assumed to obey the equation

$$\left(\frac{\partial}{\partial t} + \boldsymbol{u}\cdot\nabla\right)\boldsymbol{w} = -\nabla q + \alpha\nabla^2\boldsymbol{w}, \tag{1.10}$$

$$\nabla\cdot\boldsymbol{w} = 0, \tag{1.11}$$

where q is the pseudopressure, introduced to ensure incompressibility of vector $\boldsymbol{w}$, and α is the pseudoviscosity. The commonalities between Eqs. Eq. (1.10), Eq. (1.11) and Navier-Stokes equation are as follows:

1. Three components in $\boldsymbol{w}$;
2. Convection by the velocity, $\boldsymbol{u}$;
3. Pseudo-pressure q, and resulting incompressibility of $\boldsymbol{w}$;
4. When α, the total pseudoenergy $\frac{1}{2}\int \boldsymbol{w}^2 d\boldsymbol{x}$ is conserved.

When compared with the governing equation for a passive scalar, the common properties are:

1. The linearity of the convective term;

2. The molecular dissipation.

In contrast to the three components of $\boldsymbol{w}$ being constrained through incompressibility, the passive scalar is free from constraints among components. It is expected that the above common properties and structure of equations will make it easier to find a physical explanation for the differences and similarities in fluctuations between the velocity and passive scalars, which should help us to gain a deeper understanding of the essence of turbulent transport.

2

Theory of Turbulence

2.1 Governing Equations

Three fields $\boldsymbol{u}$, $\boldsymbol{w}$, θ are considered in the cubic box with size L. Three fields are assumed to be in a turbulent state which is statistically homogenuous isotropic. Velocity $\boldsymbol{u}(\boldsymbol{x},t)$, passive vector $\boldsymbol{w}(\boldsymbol{x},t)$ and passive scalar $\theta(\boldsymbol{x},t)$ are assumed to be governed by following equations

$$(\frac{\partial}{\partial t}+\boldsymbol{u}\cdot\nabla)\boldsymbol{u} = -\nabla p+\nu\nabla^2\boldsymbol{u}+\boldsymbol{f}_u, \tag{2.1}$$

$$\nabla\cdot\boldsymbol{u} = 0, \tag{2.2}$$

$$(\frac{\partial}{\partial t}+\boldsymbol{u}\cdot\nabla)\boldsymbol{w} = -\nabla q+\alpha\nabla^2\boldsymbol{w}+\boldsymbol{f}_w, \tag{2.3}$$

$$\nabla\cdot\boldsymbol{w} = 0, \tag{2.4}$$

$$(\frac{\partial}{\partial t}+\boldsymbol{u}\cdot\nabla)\theta = \kappa\nabla^2\theta+f_\theta, \tag{2.5}$$

respectively, where $p = P/\rho$ dontes pressure $P(\boldsymbol{x},t)$ normalized by density of fluid ρ , $q(\boldsymbol{x},t)$ the pseudo-pressure, ν the kinetic visocity, α the pseudo viscosity, κ the diffusion coeffecient for θ, $\boldsymbol{f}_u$, $\boldsymbol{f}_w$, and f_θ are the external forcings for $\boldsymbol{u}$, $\boldsymbol{w}$, θ, respectively. It is chosen the Schmidt number $Sc_w = \nu/\alpha$ and $Sc_\theta = \nu/\kappa$ to be unity in present study. The boundary conditions are periodic in three dimensions with the periodicity L.

2.2 Conversation Laws

When the viscosity vanishes ($\nu = 0$) and the external forcing ($f_i^u = 0$) is abscent, multiplying Eq. (2.1) by u_i and integrating over the fundamental box V, when the incompressibility $\partial_j u_j = 0$ and the Gauss's theorem are used,

$$\begin{aligned}\frac{d}{dt}\int \frac{1}{2}u^2 dV &= -\int_V \left[u_i u_j \partial_j u_i + u_i \partial_i p\right] dS \\ &= -\frac{1}{2}\int_A u^2 \boldsymbol{u}\cdot\boldsymbol{n} dS - \int_A p\boldsymbol{u}\cdot\boldsymbol{n} dS = 0, \end{aligned} \tag{2.6}$$

where S is the surface of the box and $\boldsymbol{n}$ is the normal vector on S. The right hand side of Eq. (2.6) vanishes because of the periodic boundary conditions. Similarly, one can also obtain

$$\frac{d}{dt}\int \frac{1}{2}w^2 dV = 0, \tag{2.7}$$

$$\frac{d}{dt}\int \frac{1}{2}\theta^2 dV = 0, \tag{2.8}$$

with conditions of $f_i^w = 0$, $\alpha = 0$, and $f^\theta = 0$, $\kappa = 0$, similarly under the statistical homogeneous. The kinetic energy, energy of passive vector and passive scalar per unit mass are defined as:

$$E_u = \left\langle \frac{\boldsymbol{u}^2}{2} \right\rangle = \frac{1}{V}\int \frac{\boldsymbol{u}^2}{2} dV, \tag{2.9}$$

$$E_w = \left\langle \frac{\boldsymbol{w}^2}{2} \right\rangle = \frac{1}{V}\int \frac{\boldsymbol{w}^2}{2} dV, \tag{2.10}$$

$$E_\theta = \left\langle \frac{\theta^2}{2} \right\rangle = \frac{1}{V}\int \frac{\theta^2}{2} dV, \tag{2.11}$$

respectively, where $\langle\ \rangle$ denotes the ensemble average. Then one can write

$$\begin{aligned}\frac{d}{dt}E_u &= \frac{d}{dt}\frac{1}{V}\int \frac{u^2}{2} dV = 0, \\ \frac{d}{dt}E_w &= \frac{d}{dt}\frac{1}{V}\int \frac{w^2}{2} dV = 0, \\ \frac{d}{dt}E_\theta &= \frac{d}{dt}\frac{1}{V}\int \frac{\theta^2}{2} dV = 0,\end{aligned}$$

for the three fields respectively, which means that the kinetic energy, energy of passive vector and passive scalar variance are conversed by the nonlinear or convective terms.

When ν, α and κ are nonzero, one can obtain the mean energy dissipation rate per unit mass $\overline{\epsilon}_u$, $\overline{\epsilon}_w$, $\overline{\epsilon}_\theta$ for $\boldsymbol{u}$, $\boldsymbol{w}$ and θ, as

$$-\frac{d}{dt}E_u = \overline{\epsilon}_u = \nu\langle(\nabla \boldsymbol{u})^2\rangle = 2\nu\langle(\mathrm{S}^u)^2\rangle = \nu\langle\boldsymbol{\omega}^2\rangle, \tag{2.12}$$

$$-\frac{d}{dt}E_w = \overline{\epsilon}_w = \alpha\langle(\nabla \boldsymbol{w})^2\rangle = 2\alpha\langle(\mathrm{S}^w)^2\rangle = \alpha\langle\boldsymbol{\zeta}^2\rangle, \tag{2.13}$$

$$-\frac{d}{dt}E_\theta = \overline{\epsilon}_\theta = \kappa\langle(\nabla \theta)^2\rangle = \kappa\langle\boldsymbol{g}^2\rangle, \tag{2.14}$$

respectively, where $\boldsymbol{\omega}$ is the vorticity, $\boldsymbol{\zeta}$ the pseudo vorticity, and $\boldsymbol{g}$ the scalar gradient, which are defined as

$$\boldsymbol{\omega} = \nabla \times \boldsymbol{u}, \tag{2.15}$$

$$\boldsymbol{\zeta} = \nabla \times \boldsymbol{w}, \tag{2.16}$$

$$\boldsymbol{g} = \nabla\theta, \tag{2.17}$$

and strain tensor S^A (A is u or w) is defined as

$$\mathrm{S}^A_{ij} = \frac{1}{2}\left(\frac{\partial A_j}{\partial x_i} + \frac{\partial A_i}{\partial x_j}\right). \tag{2.18}$$

The last equalities of Eq. (2.12) and Eq. (2.13) are due to the statistical isotropy. In what follows, we simply call E_u, E_w, E_θ as the energy and ϵ_u, ϵ_w, ϵ_θ as the dissipation rate, except stated explicitly.

2.3 Fourier Transform, Energy spectral, Lin's Equation and Enstropy

Here, Fourier transform of $A(\boldsymbol{x}, t)$ is defined as

$$A(\boldsymbol{k}, t) = \mathcal{F}\left[A(,t)\right] = \frac{1}{V}\int A(,t)e^{i\boldsymbol{k}\cdot\boldsymbol{x}}d\boldsymbol{x} \tag{2.19}$$

and the inverse Fourier transform as

$$A(\boldsymbol{x}, t) = \mathcal{F}^{-1}\left[A(\boldsymbol{k}, t)\right] = \int A(\boldsymbol{k}, t)e^{i\boldsymbol{k}\cdot\boldsymbol{x}}d\boldsymbol{k}, \tag{2.20}$$

respectively. The evolution equations of $\boldsymbol{u}$, $\boldsymbol{w}$, θ can be transformed as

$$\frac{\partial}{\partial t}\boldsymbol{u}(\boldsymbol{k},t) + \nu k^2 \boldsymbol{u} = \mathrm{P}_{ij}(\boldsymbol{k}) : \boldsymbol{N}^u(\boldsymbol{k},t), \tag{2.21}$$

$$\boldsymbol{N}^u(\boldsymbol{k},t) = \mathcal{F}\left[(\boldsymbol{u}\times\boldsymbol{\omega})\right], \tag{2.22}$$

$$\frac{\partial}{\partial t}\boldsymbol{w}(\boldsymbol{k},t) + \alpha k^2 \boldsymbol{w} = \mathrm{P}_{ij}(\boldsymbol{k}) : \boldsymbol{N}^w(\boldsymbol{k},t), \tag{2.23}$$

$$\boldsymbol{N}^w(\boldsymbol{k},t) = \mathcal{F}\left[-(\boldsymbol{u}\cdot\nabla)\boldsymbol{w}\right], \tag{2.24}$$

$$\frac{\partial}{\partial t}\theta(\boldsymbol{k},t) + \kappa k^2\theta - \kappa k^2\theta(\boldsymbol{k},t) = N^\theta(\boldsymbol{k},t), \tag{2.25}$$

$$N^\theta(\boldsymbol{k},t) = \mathcal{F}\left[-(\boldsymbol{u}\cdot\nabla)\theta\right], \tag{2.26}$$

where $\mathrm{P}_{ij}(\boldsymbol{k}) = \delta_{ij} - \frac{k_i k_j}{k^2}$ is the projection operator and the pressure term (pseudo-pressure term) is elimated by using the continuous equation.

The averaged energy density $Q(\boldsymbol{k},t)$ is defined as

$$Q_u(\boldsymbol{k},t) = \langle \boldsymbol{u}(\boldsymbol{k},t)\cdot\boldsymbol{u}^*(\boldsymbol{k},t)\rangle \tag{2.27}$$

$$= Q_u(k,t) \tag{2.28}$$

where A^* denotes the conjugation of complex number A, and the statistical isotropy is used in the second line. Then the kinetic energy spectrum is defined as

$$E_u(t) = \frac{1}{2}\langle \boldsymbol{u}^2\rangle = \frac{3}{2}u_0^2 = \int_0^\infty E_u(k,t)dk = \int_0^\infty 2\pi k^2 Q_u(k,t)dk, \tag{2.29}$$

so that

$$E_u(k,t) = 2\pi k^2 Q_u(k,t). \tag{2.30}$$

Similar to this, the spectra of the pseudo kinetic energy and the scalar variance are defined as

$$E_w(t) = \frac{1}{2}\langle \boldsymbol{w}^2\rangle = \frac{3}{2}w_0^2 = \int_0^\infty E_w(k,t)dk = \int_0^\infty 2\pi k^2 Q_w(k,t)dk, \tag{2.31}$$

$$E_\theta(t) = \frac{1}{2}\langle \boldsymbol{\theta}^2\rangle = \frac{1}{2}\theta_0^2 = \int_0^\infty E_\theta(k,t)dk = \int_0^\infty 2\pi k^2 Q_\theta(k,t)dk, \tag{2.32}$$

$$E_w(k,t) = 2\pi k^2 Q_w(k,t) = 2\pi k^2\langle \boldsymbol{w}(\boldsymbol{k},t)\cdot\boldsymbol{w}^*(\boldsymbol{k},t)\rangle, \tag{2.33}$$

$$E_\theta(k,t) = 2\pi k^2 Q_\theta(k,t) = 2\pi k^2\langle \theta(\boldsymbol{k},t)\theta^*(\boldsymbol{k},t)\rangle. \tag{2.34}$$

Substituting to Eq. (2.30), one can write the time evolution equation of the spectra, as

$$\frac{d}{dt}E_u(k,t) + 2\nu k^2 E_u = T_u(k,t), \tag{2.35}$$

$$\frac{d}{dt}E_w(k,t) + 2\alpha k^2 E_w = T_w(k,t), \tag{2.36}$$

$$\frac{d}{dt}E_\theta(k,t) + 2\kappa k^2 E_\theta = T_\theta(k,t), \tag{2.37}$$

which is so-called the Lin's equation for the energy spectra, and the energy transfer function $T_A(k)$ is defined as

$$T_u(k,t) = \Re\left[\int_{|\boldsymbol{k}|=k} \{\mathrm{P}(\boldsymbol{k}) : \boldsymbol{N}_u(\boldsymbol{k},t)\} \cdot \boldsymbol{u}^*(\boldsymbol{k},t) dS\right], \tag{2.38}$$

$$T_w(k,t) = \Re\left[\int_{|\boldsymbol{k}|=k} \{\mathrm{P}(\boldsymbol{k}) : \boldsymbol{N}_w(\boldsymbol{k},t)\} \cdot \boldsymbol{w}^*(\boldsymbol{k},t) dS\right], \tag{2.39}$$

$$T_\theta(k,t) = \Re\left[\int_{|\boldsymbol{k}|=k} N_\theta(\boldsymbol{k},t)\theta^*(\boldsymbol{k},t) dS\right], \tag{2.40}$$

where $\Re$ denotes the real part of a complex number. The $T_A(k)$ denotes nonlinear transfer for $E_A(k)$ from shell to shell via the nonlinear action and pressure.

The transfer flux $\Pi_u(k,t)$ which is the total amount of the kinetic energy transferred to the wave numbers k' larger than k ,

$$\Pi_u(k,t) = \int_k^\infty T_u(k',t) dk'. \tag{2.41}$$

The conversation of the kinetic energy by the convective and pressure term yields

$$\int_0^\infty T_u(k',t) dk' = 0, \tag{2.42}$$

therefore,

$$\Pi_u(k,t) = -\int_0^k T_u(k',t) dk' = \int_k^\infty T_u(k',t) dk'. \tag{2.43}$$

Integrating Eq. (2.35), one can write

$$\bar{\epsilon}_u(t) = -\frac{d}{dt}E_u(t) = -\frac{d}{dt}\int_0^\infty E_u(k,t) dk = \int_0^\infty 2\nu k^2 E_u(k,t) dk. \tag{2.44}$$

Similarly,

$$\Pi_w(k,t) = \int_k^\infty T_w(k',t)dk' = -\int_0^k T_w(k',t)dk', \tag{2.45}$$

$$\Pi_\theta(k,t) = \int_k^\infty T_\theta(k',t)dk' = -\int_0^k T_\theta(k',t)dk', \tag{2.46}$$

$$\bar{\epsilon}_w(t) = \int_0^\infty 2\alpha k^2 E_w(k,t)dk, \tag{2.47}$$

$$\bar{\epsilon}_\theta(t) = \int_0^\infty 2\kappa k^2 E_\theta(k,t)dk. \tag{2.48}$$

For later argument, we define the enstropy in three dimensional turbulence as

$$\Omega_u = \langle|\boldsymbol{\omega}|^2\rangle = \frac{\bar{\epsilon}_u}{\nu}, \tag{2.49}$$

which is not conserved for the case $\nu = 0$ and $f_i^u = 0$, and evolves according to

$$\frac{d}{dt}\Omega_u = 2\langle\omega_i \mathrm{S_{ij}} \omega_\mathrm{j}\rangle - 2\nu\langle(\nabla\boldsymbol{\omega})^2\rangle. \tag{2.50}$$

The first term of the r.h.s. is the source term which illustrates that vorticity is excite by the shear strain.

The definition of w-enstropy and θ-enstropy are written as

$$\Omega_\theta = \langle|\boldsymbol{g}|^2\rangle = \frac{\bar{\epsilon}_\theta}{\kappa}, \tag{2.51}$$

$$\Omega_w = \langle|\boldsymbol{\zeta}|^2\rangle = \frac{\bar{\epsilon}_w}{\alpha}, \tag{2.52}$$

the evolution equations can be derivated as

$$\frac{d}{dt}\Omega_\theta = -2\langle g_i \mathrm{S_{ij}} \mathrm{g_j}\rangle - 2\kappa\langle(\nabla \mathrm{g})^2\rangle, \tag{2.53}$$

$$\frac{d}{dt}\Omega_w = 2\langle\zeta_i \mathrm{S_{ij}}\zeta_\mathrm{j}\rangle + 2\langle\epsilon_\mathrm{ijk}\zeta_\mathrm{i}(\partial_\mathrm{j}\mathrm{u_l})(\partial_\mathrm{k}\mathrm{w_l})\rangle - 2\alpha\langle(\nabla\boldsymbol{\zeta})^2\rangle, \tag{2.54}$$

ϵ_{ijk} is the Levi-Civita symbol, and the first term of r.h.s. of Eq. (2.53) and Eq. (2.50) are similar to that in Eq. (2.50) illustrating the excitation by the shear strain, the second term of the r.h.s of Eq. (2.54) represent the disaligment of $\boldsymbol{\zeta}$ vector with respect to the straining motion of fluid.

2.4 von Kárman-Howarth Equations and Kolmogorov's 4/5 Laws

In this section, von Kárman-Howarth theory and Kolmogorov's theory for turbulence which are fundamental and milestone in the turbulence reseach are explained, then the application of the theories to passive scalar by Yaglom and Obukhov-Corrison is described. Further extension to the passive vector made by the present study is given later.

The longitudinal correlations of the velocity in the homogenuous isotropic turbulence are defined as

$$u_0^2 f^{uu}(r) = \langle u_L(\boldsymbol{x}+\boldsymbol{r}) u_L(\boldsymbol{x}) \rangle, \tag{2.55}$$

$$u_0^3 h^{uuu}(r) = \langle u_L(\boldsymbol{x}+\boldsymbol{r}) u_L(\boldsymbol{x}+\boldsymbol{r}) u_L(\boldsymbol{x}) \rangle, \tag{2.56}$$

where u_L is the parallel components of $\boldsymbol{u}$ to $\boldsymbol{r}$, and u_0 is the root mean square values of $\boldsymbol{u}$. With the assumption of the statistical homogeneity and isotropy (see Appendix A for the derivations), the von Kárman-Howarth equations can be derived as follows:[36]

$$\frac{\partial}{\partial_t} u_0^2 f^{uu}(r) = \left(\frac{\partial}{\partial r} + \frac{4}{r} \right) u_0^3 h^{uuu}(r) + 2\nu \left(\frac{\partial^2}{\partial r^2} + \frac{4}{r} \frac{\partial}{\partial r} \right) u_0^2 f^{uu}(r), \tag{2.57}$$

which is considered as the most import analytical result on homogenuous isotropic turbulence.

Considering the velocity increment $\delta u_i(\boldsymbol{x}, \boldsymbol{r})$ which is defined by

$$\delta u_i(\boldsymbol{x}, \boldsymbol{r}) = u_i(\boldsymbol{x}+\boldsymbol{r}) - u_i(\boldsymbol{x}), \tag{2.58}$$

one can write the relation between increment and correlation function,

$$\langle \delta u_i(\boldsymbol{r}) \delta u_i(\boldsymbol{r}) \rangle = 2 \left(Q_{ii}(0) - Q_{ii}(\boldsymbol{r}) \right), \tag{2.59}$$

$$\langle \delta u_i(\boldsymbol{r}) \delta u_j(\boldsymbol{r}) \delta u_i(\boldsymbol{r}) \rangle = 2 Q_{iij}(\boldsymbol{r}) + 4 Q_{iji}(\boldsymbol{r}), \tag{2.60}$$

where

$$Q_{ij}(\boldsymbol{r}) = \langle u_i(\boldsymbol{x}) u_j(\boldsymbol{x}+\boldsymbol{r}) \rangle = u_0^2 \left[f^{uu}(r) \delta_{ij} + \frac{r}{2} \frac{df^{uu}}{dr} \mathrm{P_{ij}(r)} \right], \tag{2.61}$$

$$\begin{aligned} Q_{ijk}(\boldsymbol{r}) &= \langle u_i(\boldsymbol{x}) u_j(\boldsymbol{x}) u_k(\boldsymbol{x}+\boldsymbol{r}) \rangle \\ &= u_0^3 \left\{ \frac{h - r\partial_r h}{2} \frac{r_i r_j r_k}{r^3} + \frac{2h + r\partial_r h}{4} \left(\frac{r_i}{r} \delta_{jk} + \frac{r_i}{r} \delta_{ik} \right) - \frac{h}{2} \frac{r_k}{r} \delta_{ij} \right\}. \end{aligned} \tag{2.62}$$

Substituting Eqs. (2.59) to (2.62), we can obtain

$$-\frac{2}{3}\overline{\epsilon}_u - \frac{1}{2}\frac{\partial}{\partial_t}S_2^u(\boldsymbol{r},t) = \frac{1}{6r^4}\frac{\partial}{\partial r}(r^4 S_3^u) - \frac{\nu}{r^4}\frac{\partial}{\partial r}(r^4\frac{\partial}{\partial r}S_2^u) \tag{2.63}$$

where

$$S_n^u(\boldsymbol{r}) = \langle(\delta_r u_L)^n\rangle \tag{2.64}$$

is the n-th order longitudinal structure function. For statistical stationary state $\frac{\partial}{\partial t} = 0$, and in the inertial range $r \gg \eta$, the last term at the right hand side can be ignored, then the Kolmogorov's 4/5 Laws is obtained as follows

$$-\frac{4}{5}\overline{\epsilon}_u r = \langle(\delta u_L)^3\rangle. \tag{2.65}$$

The von Kármán-Howarth type equation for the passive scalar θ and the passive vector $\boldsymbol{w}$ can also be derivated in the same way and,

$$\frac{\partial}{\partial_t}w_0^2 f^{ww}(r) = \frac{2}{r}u_0 w_0^2\left[h^{uww}(r) + 2q^{uww}(r)\right] + 2\alpha\left(\frac{\partial^2}{\partial r^2} + \frac{4}{r}\frac{\partial}{\partial r}\right)w_0^2 f^{ww}(r), \tag{2.66}$$

$$\frac{\partial}{\partial_t}\theta_0^2 f^{\theta}(r) = 2u_0\theta_0^2\left(\frac{\partial}{\partial r} + \frac{2}{r}\right)h^{u\theta\theta}(r) + 2\kappa\left(\frac{\partial^2}{\partial r^2} + \frac{2}{r}\frac{\partial}{\partial r}\right)\theta_0^2 f^{\theta}(r), \tag{2.67}$$

respectively. The correlation functions are defined as

$$w_0^2 f^{ww}(r) = \langle w_L(\boldsymbol{x}+\boldsymbol{r})w_L(\boldsymbol{x})\rangle, \tag{2.68}$$

$$\theta_0^2 f^{\theta\theta}(r) = \langle\theta(\boldsymbol{x}+\boldsymbol{r})\theta(\boldsymbol{x})\rangle, \tag{2.69}$$

$$u_0 w_0^2 h^{uww}(r) = \langle u_L(\boldsymbol{x}+\boldsymbol{r})w_L(\boldsymbol{x}+\boldsymbol{r})w_L(\boldsymbol{x})\rangle, \tag{2.70}$$

$$u_0 w_0^2 q^{uww}(r) = \langle u_L(\boldsymbol{x}+\boldsymbol{r})w_T(\boldsymbol{x}+\boldsymbol{r})w_T(\boldsymbol{x})\rangle, \tag{2.71}$$

$$u_0\theta_0^2 h^{u\theta\theta}(r) = \langle u_L(\boldsymbol{x}+\boldsymbol{r})\theta(\boldsymbol{x}+\boldsymbol{r})\theta(\boldsymbol{x})\rangle, \tag{2.72}$$

where w_T is one of the transverse components to $\boldsymbol{r}$ of $\boldsymbol{w}$. Then using the structure functions of increment, Yaglom's 4/3 law[7] can be written as follows,

$$-\frac{4}{3}\overline{\epsilon}_w r = \langle(\delta u_L)|\delta\boldsymbol{w}|^2\rangle, \tag{2.73}$$

$$-\frac{4}{3}\overline{\epsilon}_\theta r = \langle(\delta u_L)(\delta\theta)^2\rangle. \tag{2.74}$$

The Eq. (2.66) was newly derivated in present study. Kolmogorov's 4/5 law is generalized to

$$-\frac{4}{3}\overline{\epsilon}_u r = \langle (\delta u_L)|\delta \boldsymbol{u}|^2 \rangle. \tag{2.75}$$

which is similar to Eq. (2.65). Conveniently, the r.h.s of Eqs. (2.73) to (2.75) are related to the energy transfer flux in the real space ,

$$\Pi_A = \langle (\delta u_L)|\delta A|^2 \rangle, \tag{2.76}$$

where A could be $\boldsymbol{u}$, $\boldsymbol{w}$ or θ, respectively.

2.5 Kolmogorov's Phenomenology on Turbulence

In 1941, A. N. Kolmogorov[2] presented a universal theory (K41 for short) for the statistical law on small scales in fully developed turbulence. This theory is based on two hypotheses for high Reynolds number turbulence as:

1. There are small spatial scales r at which the turbulence is statistically homogenuous and isotropic. At these scales, the PDFs (P_n) of n-points correlations for increment of velocity $\delta_r u$ are only determined by the averaged energy dissipation rate $\overline{\epsilon}_u$ and kinetic viscosity ν.

2. When distance of points $|\boldsymbol{r}_\alpha|$, $|\boldsymbol{r}_\alpha| - |\boldsymbol{r}_\beta|$ ($\alpha \neq \beta$) are sufficiently larger than the viscous length scale η, P_n is only determined $\overline{\epsilon}_u$ and independent on ν.

On the first hypothesis, the dimensional analysis yields the scales of length, velocity and time as

$$\eta = \nu^{3/4}\overline{\epsilon}^{-1/4}, \qquad u_\eta = \nu^{1/4}\overline{\epsilon}^{1/4}, \qquad \tau_u = \nu^{1/2}\overline{\epsilon}^{-1/2}, \tag{2.77}$$

which are so-called Kolmogorov's length, velocity and time. When the Reynolds number is formed in terms of the Kolmogorov's variables, we obtain

$$Re_\eta = \frac{u_\eta \eta}{\nu} = 1, \tag{2.78}$$

meaning that at the Kolmogorov's scales the effect of viscosity balances with the nonlinear effect.

On the second hypothesis, there exists the range $\eta \ll r \ll L$, which is called the inertial range such that

$$\langle |\delta_r \boldsymbol{u}|^2 \rangle = C_2 (\bar{\epsilon} r)^{2/3}, \quad \langle |\delta_r \boldsymbol{u}|^p \rangle \propto (\bar{\epsilon} r)^{p/3}. \tag{2.79}$$

In the inertial range the energy transfer betweens scales is only via the non-linear terms. On the other hand, the range of scales which are smaller than Kolmogorov's length scale, is so-called dissipation range, and fluctuations are dominated by the viscosity term. The kinetic energy spectrum in the inertial range is written as

$$E_u(k) = C_K \bar{\epsilon}_u^{2/3} k^{-5/3}. \tag{2.80}$$

Eq. (2.80) is also called as Kolmogorov's spectrum, and is checked by experiments and simulations.

This phenomenology is also extended on the passive scalars, by Obukhov, Corrsin and Batchelor, with Batchelor's microscale scales for the first assumption of K41,

$$\eta_\theta = Sc_\kappa^{-1/2} \eta, \qquad \theta_\eta = \bar{\epsilon}_\theta^{1/2} \tau_\theta^{1/2}, \qquad \tau_\theta = \tau_u, \tag{2.81}$$

where $Sc_\kappa = \nu/\kappa$ and energy spectrum of passive scalar variance at inertial-convective range such that $max(\eta, \eta_\theta) \ll r \ll min(L_u, L_\theta)$ can be written

$$E_\theta(k) = C_{OC} \bar{\epsilon}_u^{-1/3} \bar{\epsilon}_\theta k^{-5/3}. \tag{2.82}$$

Eq. (2.82) is also checked by experiments and simulations.

The present study also extends them to the case of the passive vector as

$$\eta_w = Sc_\alpha^{-1/2} \eta, \qquad w_\eta = \bar{\epsilon}_w^{1/2} \tau_w^{1/2}, \qquad \tau_w = \tau_u, \tag{2.83}$$

where $Sc_\alpha = \nu/\alpha$. The energy spectrum of the pseudo kinetic energy at inertial-convective range can be written as

$$E_w(k) = C_{PV} \bar{\epsilon}_u^{-1/3} \bar{\epsilon}_w k^{-5/3}, \tag{2.84}$$

which will be checked with result of DNSs.

2.6 Intermittency in Turbulences

After K41 was published, it was criticized by Landau[37] on that the energy dissipation rate of turbulence in reality is not constant but fluctuates. Therefore, $\overline{\epsilon}^{\alpha}$ should be replaced by $\langle \epsilon^{\alpha} \rangle$. This requires another statistical law of ϵ. In turbulence, it is well known that the small scale quantities such as $\frac{\partial u_i}{\partial x_i}$, $\frac{\partial u_i}{\partial t}$ and so on fluctuate strongly. That extreme events occur suddenly after long time low level fluctuations, which is called as Intermittency. These phenomena also applies to the dissipation rate.

On response to Landau's criticism, Kolmogorov proposed a modification of his theory,[38] now known as K62, which includes the effect of the fluctuation effect of the dissipation rate. The detail of the theory can be found in standard text books of turbulence, e.g. Frisch,[39] Gotoh,[40] and here we describe the most relevant parts of the theory in the present study. On K41, the n-th order moments follow the nomal power law $\langle |\delta_r u_L|^p \rangle \propto r^{n/3}$, but in K62, $\langle |\delta_r u_L|^p \rangle \propto r^{\xi_p}$, and ξ_p is not a linear fluctuation of p but a non-decreasing fluctuation p as seen in Fig. 1.2. Many experiments and large scale numerical simulations show that the exponents are smaller than $p/3$, indeed, a non-decreasing fluctuation of n.

With different assumptions of distribution function of energy dissipation rate, several models of scaling exponents was suggested, e.g. $P(\ln\epsilon) \propto \mathrm{e}^{\mathrm{A}(\ln\epsilon)^{-2}}$ by Kolmogorov leads to

$$\xi^u(n) = \frac{n}{3} - \frac{\chi}{18} n(n-3), \tag{2.85}$$

where χ is a universal constant and discribes the spatial correlation of energy dissipation rate. Another well-known model was given by Z. S. She and E. Lévêque[41] in 1994, written as

$$\xi^u(n) = \frac{n}{9} + 2\left[1 - \left(\frac{2}{3}\right)^{n/3}\right] \tag{2.86}$$

It is known that passive scalar is more intermittent than velocity field, and the scaling exponents more scatter, as shown in Fig. 1.3. And it will be investigated the case of passive vector, and discussed why passive scalar is more intermittent than velocity field with comparisons of them in present study.

3

Numerical Simulations

3.1 Schemes, Initial Conditions and Forcing

On the calculation of spatial derivatives, the pseudo-spectral method using the 3D Fast Fourier Transform (FFT) with two dimensional domain decompositon parallelized was used. As it is known that when direct sum for the convolution ($\mathcal{F}[A(\boldsymbol{x})B(\boldsymbol{x})]$) takes $\mathcal{O}[N^{2\mathcal{D}}]$ operations so that it is very inefficient. To compute the convolution sum effciently, $A(\boldsymbol{k})$ and $B(\boldsymbol{k})$ are transformed back into the real space, multiplying them and again Fourier transformed to the $\boldsymbol{k}$-space. This requires $\mathcal{O}[N^{\mathcal{D}} log_2 N]$, in $\mathcal{D}$-dimensional space operation, i.e.

$$[AB](\boldsymbol{k}) = \mathcal{F}\left[\mathcal{F}^{-1}\left[A(\boldsymbol{k})\right]\mathcal{F}^{-1}\left[B(\boldsymbol{k})\right]\right]. \tag{3.1}$$

To avoid the aliasing error, Fourier modes at $k > k_{cut}$ in k-space are truncated, and we chose $k_{cut} = 2\sqrt{2}/3$ in this study.

The simulation code was written with FORTRAN language, and parallelized with MPI and openMP. The computations were mostly carried out on the Plasma Simulator at the National Institute of Fusion Science (NIFS), Toki, Japan. Pseudo-spectral method for spatial derivatives and 4th order Runge-Kutta-Gill Scheme for time integration were applied and visualizations were performed with ParaView.

The initial conditions are chosen as to be Gaussian random multivariate for all of $\boldsymbol{u}$, $\boldsymbol{w}$ and θ with the energy spectrum as

$$E_A(k, t=0) = N_A k_0^{-5} k^4 e^{-2(k/k_0)^2}, \tag{3.2}$$

where N_A denotes the normalization constant and k_0 for the wave number of the spectrum peak.

Two types of forcing are used. One is the white Gaussian random forcing with zero mean values. Their correlation functions are given as

$$\left\langle f_i^u(\boldsymbol{k},t) f_j^u(-\boldsymbol{k},s)\right\rangle = \frac{F_0^u(k)}{2\pi k^2}\mathrm{P_{ij}(k)}\delta(\mathrm{t-s}), \tag{3.3}$$

$$\left\langle f_i^w(\boldsymbol{k},t) f_j^w(-\boldsymbol{k},s)\right\rangle = \frac{F_0^w(k)}{2\pi k^2}\mathrm{P_{ij}(k)}\delta(\mathrm{t-s}), \tag{3.4}$$

$$\left\langle f^\theta(\boldsymbol{k},t) f^\theta(-\boldsymbol{k},s)\right\rangle = \frac{F_0^\theta(k)}{2\pi k^2}\delta(t-s), \tag{3.5}$$

$$F_0^A(k) = \begin{cases} \dfrac{\varepsilon_{\mathrm{inj}}^A}{k_{f_{\max}} - k_{f_{\min}}}, & \text{for } \ k_{f_{\min}} \le k < k_{f_{\max}} \\ 0, & \text{otherwise} \end{cases}, \tag{3.6}$$

where A denotes for u, w or θ, repsectively. In the stationary state ε_{inj}^A is equal to the value of the mean energy dissipation rate $\overline{\epsilon}_A$. Another type of forcing is the negative-viscous forcing, which is proportional to the fields at low band as

$$\boldsymbol{f}^u(\boldsymbol{k},t) = c_u(t)G(k)\boldsymbol{u}(\boldsymbol{k},t), \tag{3.7}$$

$$\boldsymbol{f}^w(\boldsymbol{k},t) = c_w(t)G(k)\boldsymbol{w}(\boldsymbol{k},t), \tag{3.8}$$

$$f^\theta(\boldsymbol{k},t) = c_\theta(t)G(k)\theta(\boldsymbol{k},t), \tag{3.9}$$

$$G(k) = \begin{cases} 1, & \text{for } \ k_{f_{\min}} \le k < k_{f_{\max}} \\ 0, & \text{otherwise} \end{cases} \tag{3.10}$$

$$c_A(t) = \frac{\varepsilon_{\mathrm{inj}}^A}{\int G(k)E_A(k,t)dk}. \tag{3.11}$$

3.2 Parameters and Characteristic Statistical Properties

All simulation runs are started from the Gaussian random intial fields with low Reynolds number and of the resolution of 256^3 grid points and integrated until a statistically steady state is attained. The decision whether or not the steady state is achieved is made by observing that the energy spectra do not change in time and that the evolution of the energy dissipation rates stay around the energy injection rates. When the Reynolds number is increased, the number of grid points is increased to 512^3, and the same operations are repeated to attain the steady state on the 1024^3 grid points. It takes longer time to attain stationary for higher Reynolds number, e.g. for Run C about 5 T_E (large eddy time) is required, and all the data in the transient period of each run is not taken into account in the present study.

The averages are taken as the volume average over the domain and/or time average only at the steady state. Their definitions are given below, and the results are listed in Table 3.1, together with the simulation parameters. Caculations of the Kolmogorov's length η is as,

$$\eta = \nu^{3/4}\overline{\epsilon}_u^{-1/4} \tag{3.12}$$

the integral length L_u, L_w, L_θ,

$$L_u = \frac{3\pi}{4}\frac{\int_0^\infty k^{-1}E_u(k)dk}{\int_0^\infty E_u(k)dk}, \tag{3.13}$$

$$L_w = \frac{3\pi}{4}\frac{\int_0^\infty k^{-1}E_w(k)dk}{\int_0^\infty E_w(k)dk}, \tag{3.14}$$

$$L_\theta = \frac{\pi}{2}\frac{\int_0^\infty k^{-1}E_\theta(k)dk}{\int_0^\infty E_\theta(k)dk}, \tag{3.15}$$

the large eddy turnover time T_E,

$$T_E = L_u/u_0 \tag{3.16}$$

Taylor's microscale lengths λ_u, λ_w, λ_θ,

$$\lambda_u = \sqrt{\frac{\langle u_1^2 \rangle}{\langle (\partial u_1/\partial x_1)^2 \rangle}} = \sqrt{15 u_0^2 \frac{\nu}{\overline{\epsilon}_u}}, \tag{3.17}$$

$$\lambda_w = \sqrt{\frac{\langle w_1^2 \rangle}{\langle (\partial w_1/\partial x_1)^2 \rangle}} = \sqrt{15 w_0^2 \frac{\alpha}{\overline{\epsilon}_w}}, \tag{3.18}$$

$$\lambda_\theta = \sqrt{\frac{\langle \theta^2 \rangle}{\langle (\partial \theta/\partial x_1)^2 \rangle}} = \sqrt{3 \theta_0^2 \frac{\kappa}{\overline{\epsilon}_\theta}}, \tag{3.19}$$

and the Taylor microscale Reynolds number R_λ:

$$R_\lambda = \frac{u_0 \lambda_u}{\nu}, \tag{3.20}$$

respectively. Skewness of derivatives S_K^u, S_K^w, S_K^θ are measures of generating of th small scales and defined as

$$S_K^u = \frac{\langle (\partial u_1/\partial x_1)^3 \rangle}{\langle (\partial u_1/\partial x_1)^2 \rangle^{3/2}}, \tag{3.21}$$

$$S_K^w = \frac{\langle (\partial u_1/\partial x_1)[(\partial w_1/\partial x_1)^2 + (\partial w_2/\partial x_1)^2 + (\partial w_1/\partial x_1)^2] \rangle}{\langle (\partial u_1/\partial x_1)^2 \rangle^{1/2} \langle (\partial w_1/\partial x_1)^2 + (\partial w_2/\partial x_1)^2 + (\partial w_1/\partial x_1)^2 \rangle}, \tag{3.22}$$

$$S_K^\theta = \frac{\langle (\partial u_1/\partial x_1)(\partial \theta/\partial x_1)^2 \rangle}{\langle (\partial u_1/\partial x_1)^2 \rangle^{1/2} \langle (\partial \theta/\partial x_1)^2 \rangle}. \tag{3.23}$$

When the turbulence is isotropic, the skewnesses are related to the transfer functions as

$$\int_0^\infty k^2 T_u(k) dk = -\frac{35}{2} \left\langle \left(\frac{\partial u_1}{\partial x_1} \right)^3 \right\rangle, \tag{3.24}$$

$$\int_0^\infty k^2 T_w(k) dl = -\frac{15}{2} S_K^w, \tag{3.25}$$

$$\int_0^\infty k^2 T_\theta(k) dl = -\frac{9}{2} S_K^\theta. \tag{3.26}$$

It is argued that the spatial resolution in DNS requires $k_{max}\eta > 1.5$ for the velocity, where k_{max} is the maxium wave number in DNS, but the resolution for the passive scalar is more demanding because of the effcient transfer of the scalar variance to high wavenumbers and strong intermittency.[15,42,43,44] Esepecially the accurate computation of the extreme values or high order moments of the

scalar gradient requires large values of $k_{max}\eta_\theta$, say greater than 5 or more,[45,44] where $\eta_\theta = \eta Sc_\kappa^{-1/2}$ is the Batchelor length. In the present DNS runs $\eta_\theta = \eta$ because $Sc_\theta = 1$, and the spatial resolution is $k_{max}\eta = 2.25, 1.14, 0.80, 1.22$ and 2.24. Run A and E meet the requirement of velocity field and all runs don't meet the requirement for the passive scalar and the passive vector. However, in this study, the concern is mostly on the statistical behavior in the inertial-convective range, therefore it is considered that as far as the scale of interests lies in the inertial-convective range, the spatial resolution in the present DNS study does not affect the analysis. Indeed it has been studied the inertial range statistics are insensitive to the dissipation range.[42]

Run E in which the forcing range is set at higher wave numbers. The purpose of the Run E is to check the statistical convergence of the one point probability density functions (PDFs). It is necessary to simulate turbulence fields which are exiceted by many Fourier modes for the forcing in order to obtain well converged PDFs.

Table 3.1: DNS parameters and characteristic statistics.

	Run A	Run B	Run C	Run D	Run E
N	1024	1024	1024	1024	1024
R_λ	194.2	300.9	397.1	300.9	87.1
$k_{\max}\eta$	2.25	1.14	0.80	1.22	2.24
$[k_{\mathrm{f_{low}}}, k_{f_{\mathrm{high}}}]$	$[2, 3]$	$[2, 3]$	$[2, 3]$	$[2, 3]$	$[6,\ 10]$
Δt	2×10^{-4}	10^{-4}	5×10^{-5}	10^{-4}	5×10^{-4}
ν	5×10^{-4}	2×10^{-4}	1.2×10^{-4}	2×10^{-4}	5×10^{-4}
T_E	0.92	0.79	0.82	0.88	0.43
T_{av}/T_E	10.31	10.58	10.29	10.02	11.68
$\overline{E}_u$	0.88	0.94	0.91	0.82	0.44
$\overline{E}_w$	0.67	0.60	0.67	0.60	0.29
$\overline{E}_\theta$	0.18	0.15	0.15	0.13	0.08
$\varepsilon^u_{\mathrm{inj}}$	0.3	0.3	0.3	0.3	0.3
$\varepsilon^w_{\mathrm{inj}}$	0.3	0.3	0.3	0.3	0.3
$\varepsilon^\theta_{\mathrm{inj}}$	0.1	0.1	0.1	0.1	0.1
$\overline{\epsilon}_u$	0.34	0.32	0.29	0.25	0.34
$\overline{\epsilon}_w$	0.32	0.30	0.33	0.26	0.34
$\overline{\epsilon}_\theta$	0.10	0.10	0.10	0.09	0.11
L_u	0.69	0.62	0.64	0.65	0.23
L_w	0.65	0.65	0.64	0.67	0.23
L_θ	0.43	0.44	0.43	0.42	0.15
λ_u	0.120	0.076	0.061	0.081	0.080
λ_w	0.097	0.063	0.050	0.068	0.065
λ_θ	0.055	0.035	0.027	0.035	0.046
C_K	1.57	1.55	1.57	1.59	n / a
C_w	0.93	1.00	1.00	1.06	n / a
C_{OC}	0.65	0.69	0.68	0.69	n / a
S^u_K	-0.54	-0.54	-0.47	-0.54	-0.51
S^w_K	-0.46	-0.41	-0.31	-0.40	-0.47
S^u_K	-0.51	-0.44	-0.34	-0.45	-0.51

4

Results

The results are presented regarding three aspects:

1. Visualization of turbulent fields. Field visualization gives an intuitive image on the three fields which help our understanding and interpretation of the statistical quantities discussed later. The geometry of $\Omega_u = (\nabla \times \boldsymbol{u})^2$ and $\Omega_\theta = (\nabla\theta)^2$ is one of the distinctive differences between turbulence velocity $\boldsymbol{u}$ and turbulent passive scalar θ. The comparison of geometry for $\Omega_w = (\nabla \times \boldsymbol{w})^2$ to others brings knowledge about the generation of tube/sheet-like structures, e.g. whether it is due to pressure (continuity) or others. The visualization for pressure p, pseudo-pressure q and their derivatives are also given.

2. Low order statistics as the second and third order moments. The time variation of the energy and dissipation rate, the spectra of the mean energy, the transfer flux, the pressure, the production of enstropy, and the 4/5 and 4/3 laws are given. The Kolmogorov constant C_K for the velocity, C_{PV} for the passive vector, and the Obukhov-Cossin constant C_{OC} for the passive scalar are computed via the compensated spectra. Band-to-band transfer are also studied to see the bottleneck effect in the energy spectrum.

3. High order statistics. The statistical properties are mainly studied via two points of view: PDFs and scaling exponents of the moments. It is known

that the long tails of PDFs and the anomalous scaling exponents are manifests of the intermittency, which is one of features of the turbulence in three dimensional space.

In Section 4.1, data of Run A is mainly used, because of the fine resolution of $k_{max}\eta = 2.25$, and a domain with size of $L/8$ is used to see the small scale structures. In Section 4.2 and Section 4.3, data of Run B are mainly used, because of larger Reynolds number, while satisfying $k_{max}\eta \sim 1.5$. Run C is chosen to examine the scaling exponents in the inertial-convective range, because that Reynolds number of Run C is highest in present study. Run D is used to check the effects of forcing method on the intermittency. Run E is used to study the one point PDFs and to compare with other runs.

4.1 Visualization

For visualization, a snapshot at an instantaneous time in the steady state and in the sub domain $x, y, z \in [0, L/8]$ is used. Quantities that are positive definite are normalized by the average value over the entire volume of current snapshot, and the quantities that are not positive definite are normalized by the root of mean square at the entire volume.

4.1.1 Enstropy, Pseudo-enstropy and Squares of Scalar Gradient

First, it is checked the spatial structure of the enstropy Ω_u (Fig. 4.1), the pseudo-enstropy Ω_w (Fig. 4.3) and squares of scalar gradient Ω_θ (Fig. 4.2), which are defined as

$$\Omega_u^{/ast}(\boldsymbol{x}, t) = \frac{(\nabla \times \boldsymbol{u})^2}{\langle (\nabla \times \boldsymbol{u})^2 \rangle}, \tag{4.1}$$

$$\Omega_w^{/ast}(\boldsymbol{x}, t) = \frac{(\nabla \times \boldsymbol{w})^2}{\langle (\nabla \times \boldsymbol{w})^2 \rangle}, \tag{4.2}$$

$$\Omega_\theta^{/ast}(\boldsymbol{x}, t) = \frac{(\nabla \theta)^2}{\langle (\nabla \theta)^2 \rangle}, \tag{4.3}$$

respectively.

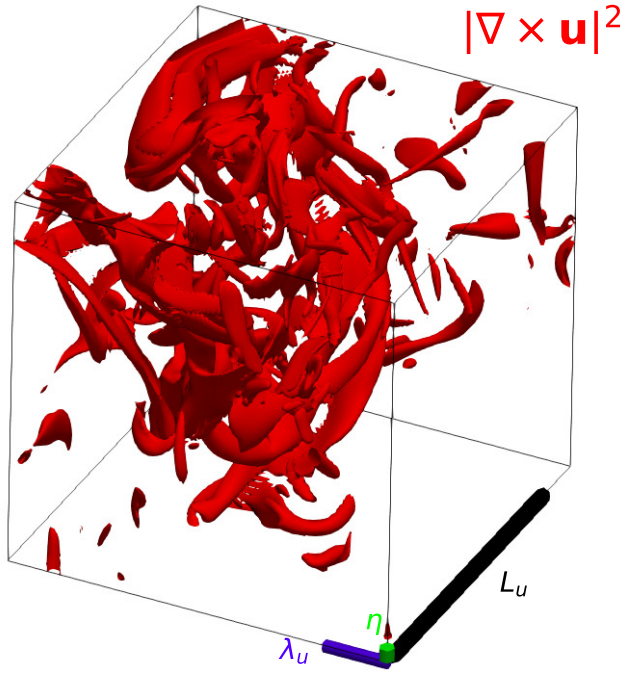

Figure 4.1: Iso-surface of square of vorticity for Run A, with level at $\Omega_u^{/ast}(\boldsymbol{x}) > 8$ in a cubic box with size of $L/8$.

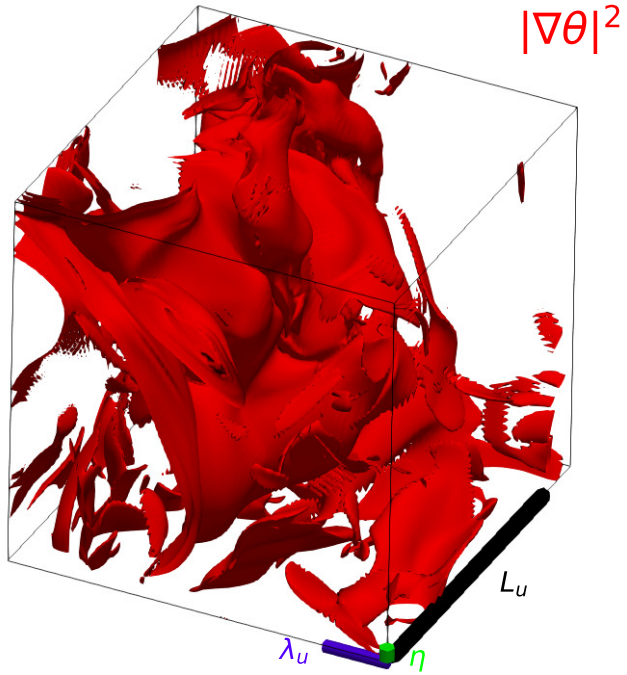

Figure 4.2: Iso-surface of square of gradient of passive scalar for run A, with level at $\Omega_\theta^{/ast}(\boldsymbol{x}) > 8$ in a cubic box with size of $L/8$.

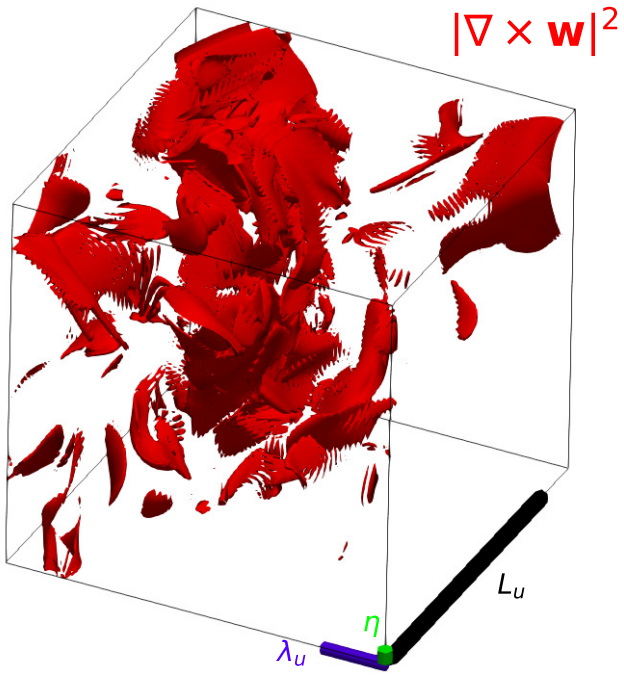

Figure 4.3: Iso-surface of square of pseudo-vorticity for run A, with level at $\Omega_w^{/ast}(\boldsymbol{x}) > 8$ in a cubic box with size of $L/8$.

The geometry of Ω_w is sheet-like. This is dissimilar to the tube-like geometry of Ω_u,[19] but similar to the sheet-like geometry of Ω_θ.[46,47,48] In the tube-like structure, the vortex lines are bundled in a circle, while in the sheet-like structure of pseudo-vortex, the vortex lines are bundled into a sheet.

The charactistic lengths for the velocity listed in Table 3.1 for Run A are:

$$\eta = 2.25/512 = 0.0044, \quad \lambda_u = 0.12, \quad L_u = 0.69. \tag{4.4}$$

It could be observed that, the radius of vortex tube for Ω_u is of the order of η, and length of order λ_u, the thickness of the vortex-sheet for Ω_w and gradient-sheet for Ω_θ is smaller than η.

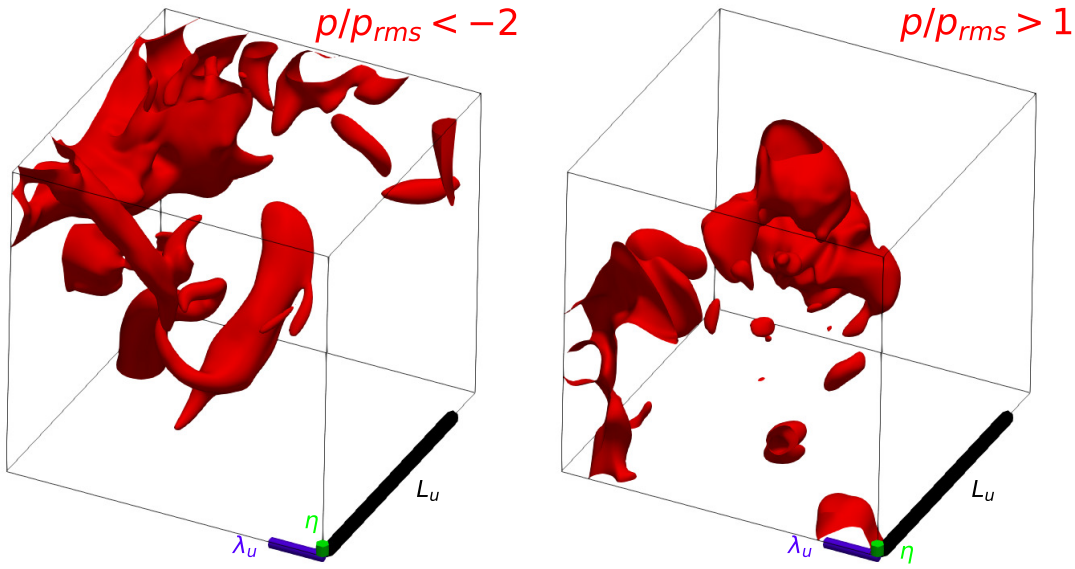

Figure 4.4: Isosurface of pressure for Run A with level of $-2p_{rms}$ (left) for negative and p_{rms} (right) for positive.

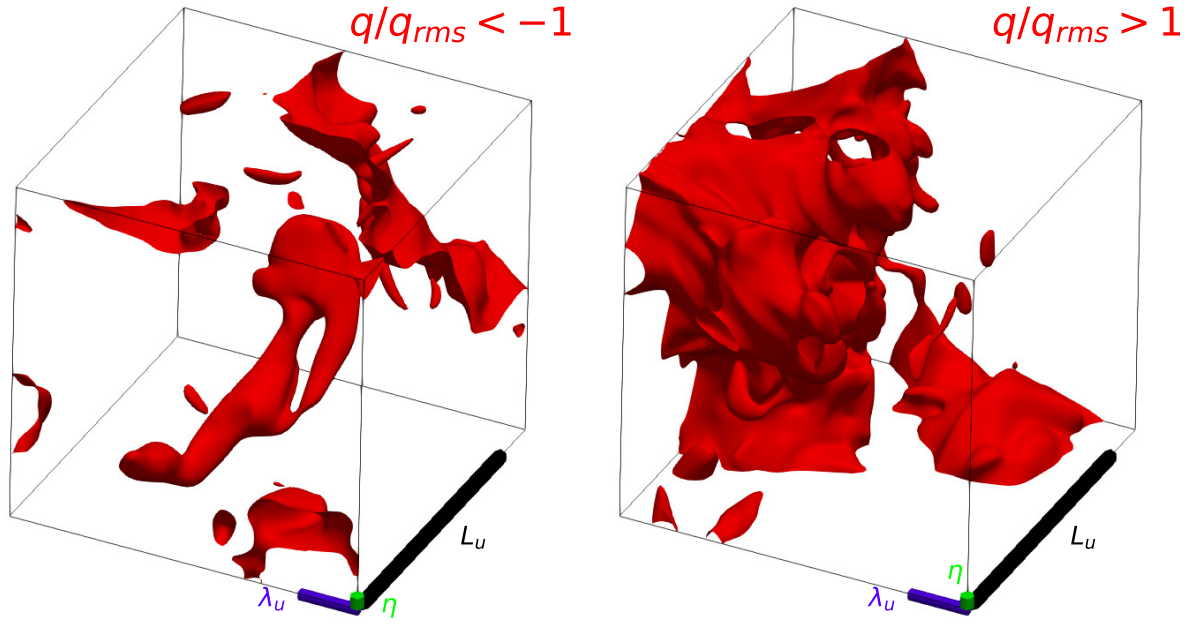

Figure 4.5: Isosurface of pseudopressure for Run A with level of $-2p_{rms}$ (left) for negative and $2p_{rms}$ (right) for positive.

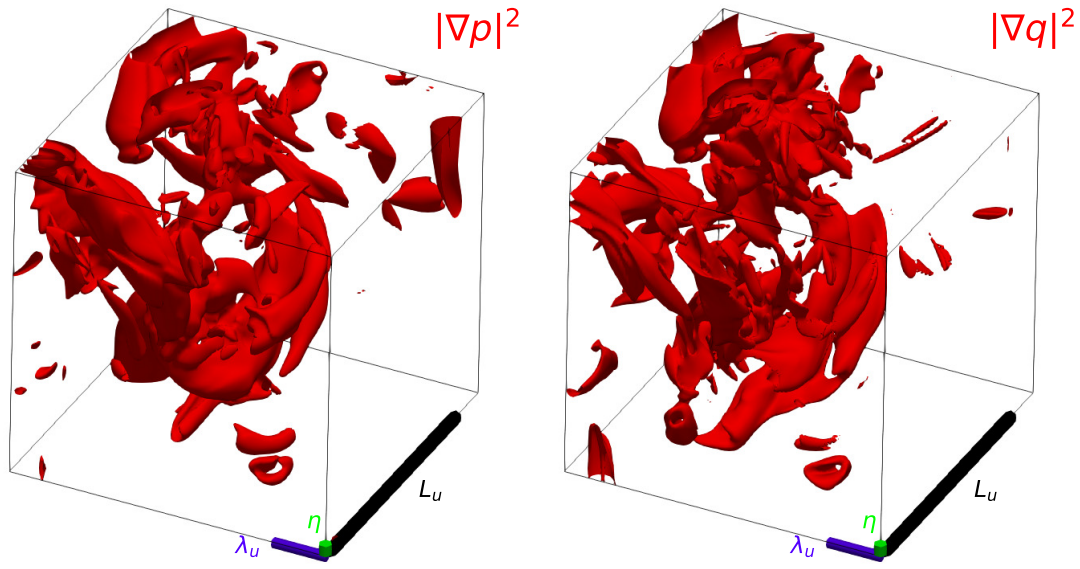

Figure 4.6: Iso-surface of Ω_p(left) and Ω_q(right) for run A, with level at $\Omega_A^{/ast}(\boldsymbol{x}) > 8$ in a cubic box with size of $L/8$.

4.1.2 Pressure and Pseudo-pressure

Pressure p (Fig. 4.4), pseudo-pressure q (Fig. 4.5) and squares of their gradient (Fig. 4.6) are also shown by the isosurfaces, with definition:

$$\Omega_p^{/ast}(\boldsymbol{x},t) = \frac{(\nabla p)^2}{\langle(\nabla p)^2\rangle}, \tag{4.5}$$

$$\Omega_q^{/ast}(\boldsymbol{x},t) = \frac{(\nabla q)^2}{\langle(\nabla q)^2\rangle}, \tag{4.6}$$

respectively.

It can be found that the geometry of the pressure for the negative part and the positive part are different to each other. The negative part is tube-like, while the positive part is blob-like. On the other hand, the isosurfaces of both the positive part and negative part of pseudo-pressure are blob-like. It is found that $|\frac{p_{min}}{p_{max}}| > |\frac{q_{min}}{q_{max}}|$, indicating that the pressure PDF is negatively skewed, which will be discussed in Section 4.3. On the geometry Ω_p and Ω_q which are shown in Fig. 4.6, both of them are tube-like, but radii of the tubes are larger than vortex tubes in Fig. 4.1.

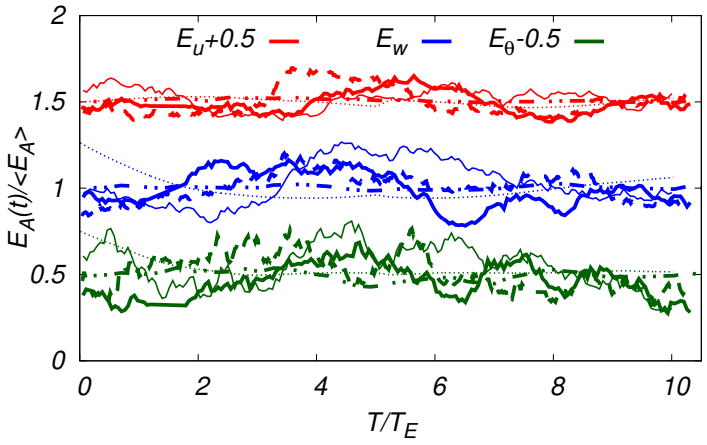

Figure 4.7: Time variation of $E_u/\overline{E_u}+0.5$, $E_w/\overline{E_w}$ and $E_\theta/\overline{E_\theta}-0.5$. Thick lines denotes for Run A, thin solid lines for Run B, broken lines for Run C, dotted lines for Run D, dotted-broken lines for Run E.

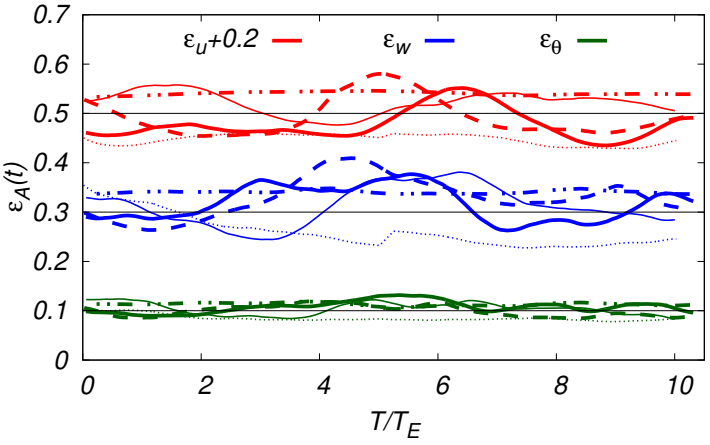

Figure 4.8: Time variation of $\epsilon_u+0.2$, ϵ_w and ϵ_θ. Line style configuration for runs is same as Fig. 4.7.

4.2 Low Order Statistics

4.2.1 Time Histories of Simulations

The time variation of the normalized energy are shown in Fig. 4.7. For ease of visibility, the curves of $E_u(t)/\overline{E}_u$ are shifted by 0.5, the curves of $E_\theta(t)/\overline{E}_\theta$ are

shifted by -0.5. The time variation of the energy dissipation rates are shown in Fig. 4.8, the curves of $\epsilon_u(t)$ are shifted by 0.2, and the energy injection rates are illustrated with straight lines. The oscillations period of the normalized energies for Run D and Run E are longer than that of Run A-C. Fluctuations of the energy dissipation rate are smaller than those of normalized energies, because that the dissipation rate reflects small scale properties and less correlates the fast variance external forcing than large scale.

4.2.2 Energy Spectra and Fluxes

Using the Kolmogorov variables, we normalize the spectra as

$$E_u^*(k\eta) = \overline{\epsilon}_u^{-1/4}\nu^{-5/4}E_u(k), \tag{4.7}$$

$$E_w^*(k\eta) = \overline{\epsilon}_w^{-2}\overline{\epsilon}_u^{3/4}\alpha^{-2}\nu^{3/4}E_w(k), \tag{4.8}$$

$$E_\theta^*(k\eta) = \overline{\epsilon}_\theta^{-2}\overline{\epsilon}_u^{3/4}\kappa^{-2}\nu^{3/4}E_\theta(k), \tag{4.9}$$

The normalized spectra are plotted in Fig. 4.9.

For ease of visibility, the curves of $E_u^*(k\eta)$ and $E_w^*(k\eta)$ are shifted by 100 and 10, respectively. All curves, including E_w^*, collapse excellently onto a single curve for $k\eta \in [0.01, 0.1]$, which indicates that an approximate -5/3 power law holds, as expected based on Kolmogorov-Obukhov-Corrsin theory. For $k\eta > 0.3$, E_w^* and E_θ^* decay slower than E_u^* meaning that E_w and E_θ are excited more strongly than E_u at large wave numbers in the dissipative range.

To compute the non-dimensional constants C_K, C_{PV} and C_{OC}, the compensated spectra for Run B

$$\psi_u(k\eta) = \overline{\epsilon}_u^{-2/3}k^{5/3}E_u(k), \tag{4.10}$$

$$\psi_w(k\eta) = \overline{\epsilon}_u^{1/3}\overline{\epsilon}_w^{-1}k^{5/3}E_w(k), \tag{4.11}$$

$$\psi_\theta(k\eta) = \overline{\epsilon}_u^{1/3}\overline{\epsilon}_\theta^{-1}k^{5/3}E_\theta(k), \tag{4.12}$$

are plotted in Fig. 4.10. The mean values of curves at plateau for $0.025 < k\eta < 0.035$[45] are found to be

$$C_K = 1.55, \qquad C_{PV} = 1.00, \qquad C_{OC} = 0.69, \tag{4.13}$$

respectively.

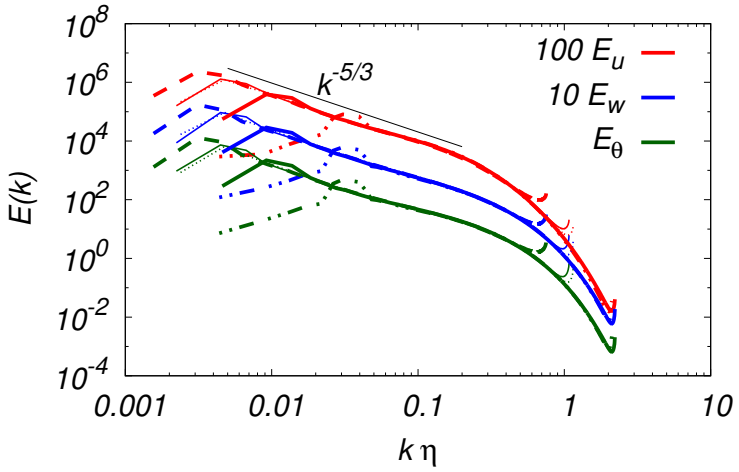

Figure 4.9: Averaged normalized spectra over the steady state for runs, the curves of $E_u^*(k)$ and $E_w^*(k)$ are shifted by 100 and 10 vertically for ease of visibility. Line style configuration for runs is same as Fig. 4.7.

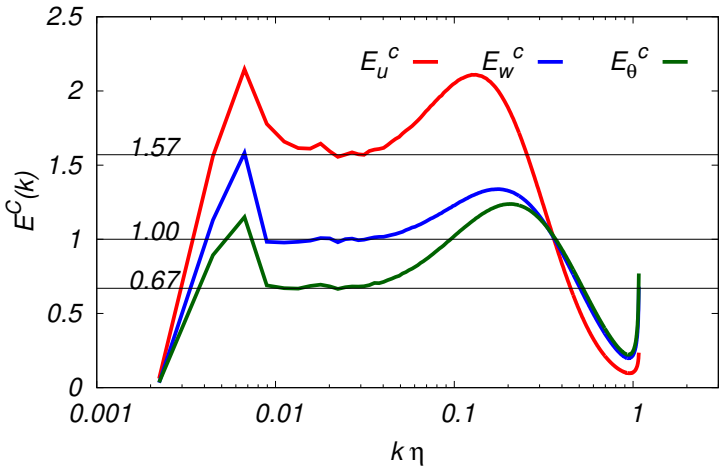

Figure 4.10: Averaged compensated spectra over the steady state for Run B. Thin black lines indicate the Kolmogorov-Obukhov-Corrsin constants calculated by the compensated spectra.

The Kolmogorov and Obukhov-Corrsin constants, $C_K = 1.55$ and $C_{OC} = 0.69$, are consistent with those in the literature.[5,15,49,50,45] In agreement with the previous studies, we observe that the spectral bump of the passive scalar is strongest and attains at higher wave numbers than the kinetic energy. The compensated spectrum of E_w shows a similar trend, but is between those of the

kinetic energy and the passive scalar. We examine the spectral bump in more detail below.

The spectra of the energy transfer fluxes normalized by the energy dissipation rates are plotted in Fig. 4.11. All of the curves are close to unity for $0.005 < k\eta < 0.03$, but the curves of Π_θ decays more slowly than Π_u, followed by Π_w in the far dissipation range. These trend are consistent with strong excitation of E_w and E_θ at high wave numbers.

4.2.3 4/5 Law and 4/3 Laws

The normalized structure functions $S_u^*(r)$, $S_w^*(r)$ and $S_\theta^*(r)$ are defined as

$$S_u^*(r) = -\frac{\langle(\delta u_L)^3\rangle}{\frac{4}{5}\overline{\epsilon}_u r}, \tag{4.14}$$

$$S_w^*(r) = -\frac{\langle(\delta u_L)|\delta w|^2\rangle}{\frac{4}{3}\overline{\epsilon}_w r}, \tag{4.15}$$

$$S_\theta^*(r) = -\frac{\langle(\delta u_L)(\delta\theta)^2\rangle}{\frac{4}{3}\overline{\epsilon}_\theta r}, \tag{4.16}$$

respectively, and shown in Fig. 4.12.

The plateaus of the three curves approach unity from below at round $r/\eta \sim 100$, indicating that Kolmogorov's 4/5 and 4/3 laws hold for S_u^* and S_w^*, and Yaglom's 4/3 law for S_θ^*, respectively. The fact that all of the S_A^* $(A = u, w, \theta)$ curves are smaller than unity is consistent with previous studies.[5,15] Careful examination reveals that the plateau of S_θ^* appears roughly in the range $20 < r/\eta < 80$ and that of S_u^* occurs at larger scales as $60 < r/\eta < 200$, while the plateau of S_w^* is in the range $40 < r/\eta < 200$, which is wider than that of the two curves. Moreover, the S_w^* curves collapses to S_θ^* in the dissipation range $r/\eta < 10$. These trends are consistent with the high excitations of $E_w(k)$ and $E_\theta(k)$ shown in Fig. 4.9, and collapse of $\Pi_w(k)$ and $\Pi_\theta(k)$ at high wave numbers in Fig. 4.11.

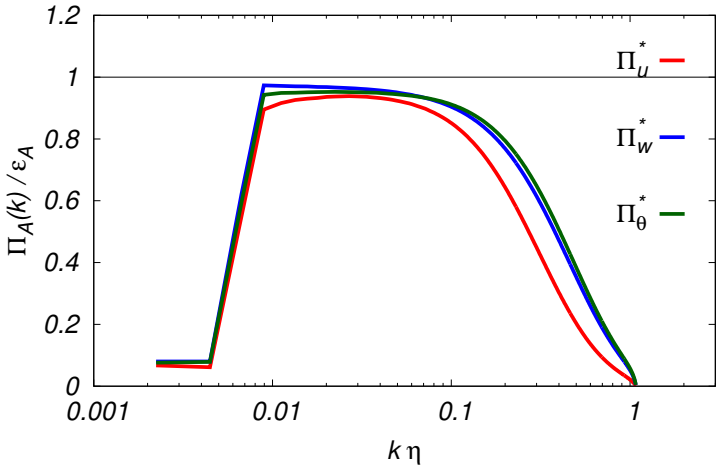

Figure 4.11: Averaged normalized energy transfer fluxes over the steady state for Run B. Red: $\Pi_u/\overline{\epsilon}_u$, blue: $\Pi_w/\overline{\epsilon}_w$, green: Red: $\Pi_\theta/\overline{\epsilon}_\theta$.

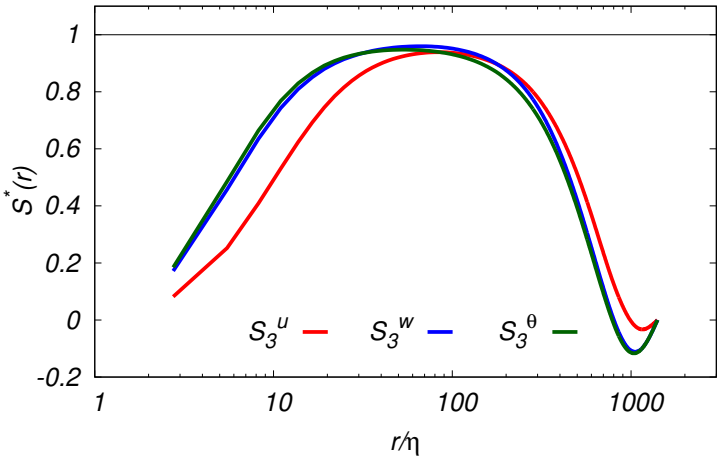

Figure 4.12: Averaged normalized 3rd order structure functions over the steady state for Run B. Red: $-\langle \delta u_L^3 \rangle / (\frac{4}{5}\overline{\epsilon}_u r)$, blue: $-\langle \delta u_L (\delta \boldsymbol{w})^2 \rangle / (\frac{4}{3}\overline{\epsilon}_w r)$, green: Red: $-\langle \delta u_L (\delta\theta)^2 \rangle / (\frac{4}{3}\overline{\epsilon}_\theta r)$.

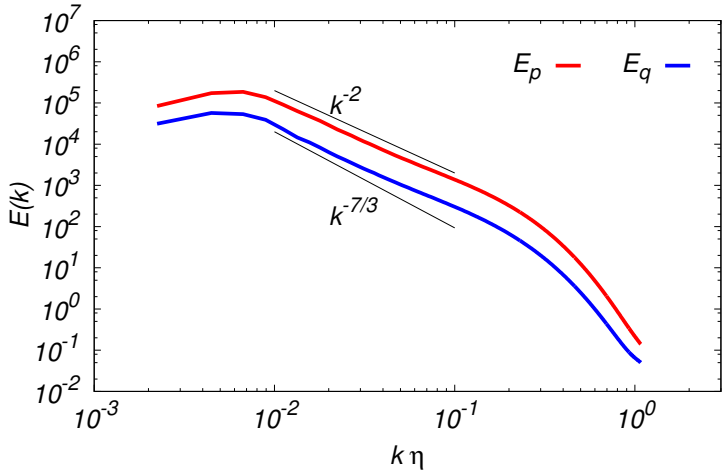

Figure 4.13: Spectra of pressure and pseudo-pressure normalized by Kolmogorov's microscales for Run B.

4.2.4 Spectra of Pressure and Pseudo-pressure

The spectra of the pressure and pseudo-pressure are defined as

$$\langle p^2 \rangle = \int_0^\infty E_p(k) dk, \tag{4.17}$$

$$\langle q^2 \rangle = \int_0^\infty E_q(k) dk, \tag{4.18}$$

respectively, and normalized in terms of the Kolmogorov variables as

$$E_p^*(k\eta) = u_\eta^{-4} \eta^{-1} E_p(k), \tag{4.19}$$

$$E_q^*(k\eta) = (u_\eta w_\eta)^{-2} \eta_w^{-1} E_q(k), \tag{4.20}$$

respectively. They are shown in Fig. 4.13 for Run B. It is observed that $E_q(k) < E_p(k)$ at all wave numbers, but the overall functional forms are very similar to each other. Both of two curves approach to the power law $E_{p,q}(k) \propto k^{-\beta}$ in the range $0.01 < k\eta < 0.1$, with the slope $\beta \simeq 2$, which slightly shallower than the $k^{-7/3}$ Kolmogorov scaling. This is due to the relatively lower Reynolds number.[51,52]

To compare E_p and E_q more closely, the compensated spectra of $E_p(k\eta)/E_p(k^*\eta)$ and $E_q(k\eta)/E_q(k^*\eta)$ ($k^*\eta = 0.03$) are shown in Fig. 4.14 and $E_p(k)/E_q(k)$ is shown

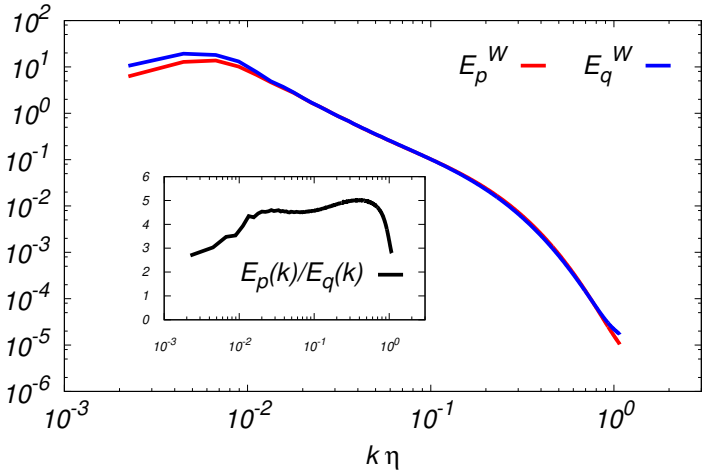

Figure 4.14: Comparison of shifted spectra of pressure by ratio to $E_p(\mathrm{k}^*)$ and $E_q(\mathrm{k}^*)$ respectively, with $\mathrm{k}^*\eta = 0.03$.

in the inset of Fig. 4.14, respectively. One can see that two curves collapse well in the range $0.015 < k\eta < 1$. The ratio is about 2 at small wavenumbers and increases quickly, reaches the maximum at round $k\eta = 0.7$, and finally falls off quickly at high wave numbers.

4.2.5 Spectra of Production of Gradients of Velocity, Passive vector and Scalar

The vorticity is enhanced by the stretching action of the turbulent flow as seen in Eqs. (2.50), (2.53) and (2.54). However, the pseudo-vorticity is not only excited by the stretching action, but also affected by the second term of right hand side of Eq. (2.54).

It is interesting to compare their strength and examine the wave number ranges that contribute to the production of vorticity, pseudo-vorticity and the

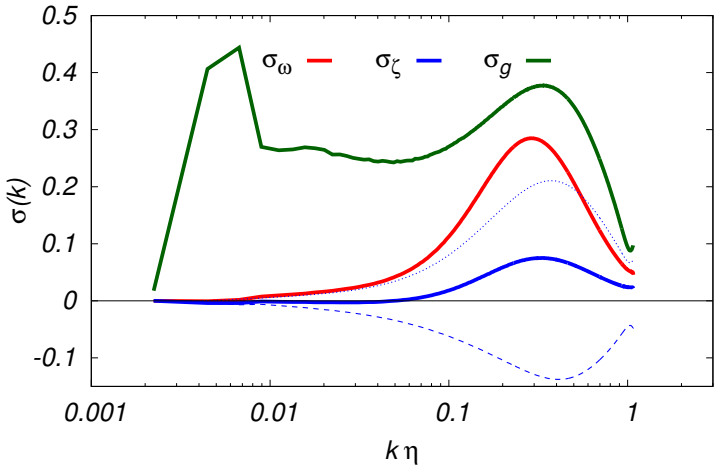

Figure 4.15: Spectra of production terms of enstropy, pseudo-enstropy and scalar gradient for Run B. Red: σ^*_ω, blue: σ^*_ζ, green: σ^*_g. The blue dotted line denotes $\sigma_{\zeta,str}$, and the blue broken line $\sigma_{\zeta,crs}$.

scalar gradient. For this purpose, following spectra are investigated:

$$\sigma^*_\omega(k) = \frac{1}{\langle \boldsymbol{\omega}^2 \rangle^{3/2} \eta} \int_{|\boldsymbol{k}|=k} \langle \boldsymbol{\omega}(-\boldsymbol{k}) \cdot \mathcal{F}[S : \boldsymbol{\omega}] \rangle dS(\boldsymbol{k}), \tag{4.21}$$

$$\sigma^*_{\zeta,str}(k) = \frac{1}{\langle \boldsymbol{\zeta}^2 \rangle \langle \boldsymbol{\omega}^2 \rangle^{1/2} \eta} \int_{|\boldsymbol{k}|=k} \langle \boldsymbol{\zeta}(-\boldsymbol{k}) \cdot \mathcal{F}[S : \boldsymbol{\zeta}] \rangle dS(\boldsymbol{k}), \tag{4.22}$$

$$\sigma^*_{\zeta,crs}(k) = \frac{1}{\langle \boldsymbol{\zeta}^2 \rangle \langle \boldsymbol{\omega}^2 \rangle^{1/2} \eta} \int_{|\boldsymbol{k}|=k} \langle \boldsymbol{\zeta}(-\boldsymbol{k}) \cdot \mathcal{F}[(\nabla \boldsymbol{u})^T \times (\nabla \boldsymbol{w})^T] \rangle dS(\boldsymbol{k}), \tag{4.23}$$

$$\sigma^*_\zeta(k) = \sigma^*_{\zeta,str}(k) + \sigma^*_{\zeta,crs}(k), \tag{4.24}$$

$$\sigma^*_g(k) = -\frac{1}{\langle \boldsymbol{g}^2 \rangle \langle \boldsymbol{\omega}^2 \rangle^{1/2} \eta} \int_{|\boldsymbol{k}|=k} \langle \boldsymbol{g}(-\boldsymbol{k}) \cdot \mathcal{F}[S : \boldsymbol{g}] \rangle dS(\boldsymbol{k}), \tag{4.25}$$

where $A^T_{ij} = A_{ji}$ denotes the transpose, and S is the surface element in the k-space with radius of k, and the result for Run B is plotted in Fig. 4.15. One could see that $\sigma_{\zeta,str}$ is positive at all the wavenumbers just like σ_ω, meaning that the production of pseudo-vorticity is due to the stretching effects by the turbulence, but $\sigma_{\zeta,crs}$ is negative and attenates the production by destroying the geometrical coherency between $\nabla \boldsymbol{u}$ and $\nabla \boldsymbol{w}$. Therefore, the total production of the pseudo-vorticity is positive, but less intensive than the vorticity production, when taking account of the normalization $\langle \boldsymbol{\omega}^2 \rangle / \langle \boldsymbol{\zeta}^2 \rangle \sim \overline{\epsilon}_u / \overline{\epsilon}_w \sim \varepsilon^u_{\rm inj} / \varepsilon^w_{\rm inj} = 1$ in this study.

The σ_ω^*, σ_ζ^* and σ_g^* are positive at all wave numbers and have peaks at $k\eta \sim 0.2$. When the wave number decreases, σ_ω^* and σ_ζ^* decay quickly for $k\eta < 0.1$ and vanish at $k\eta < 0.01$, but σ_g^* remains finite. Although we are not successful to explain why σ_g is finite at low wavenumbers, it is noted that in DNSs and experiments the ramp-cliff or masa-canyon structure of the scalar field accompanied with large scalar gradients is found to have very large scale structures of integral length or larger scales.[53,15,20,24,54,55]

4.2.6 Bottleneck Effects and Band-to-Band Transfer

One way to compare the amplitudes of the spectral bumps of $E_u(k)$, $E_w(k)$ and $E_\theta(k)$ on an equal footing is to divide the compensated spectra by their plateau values, the Kolmogorov constants C_K, C_{PV}, and the Obukhov-Corrsin constant C_{OC}, respectively. The resulting curves are plotted in Fig. 4.16. The peak values indicate the bump amplitude with respect to the plateau level. The wave numbers and values of the bump maximum of the curve are denoted k_p^u, k_p^w, k_p^θ and A_p^u, A_p^w, A_p^θ, respectively. The results from Run B are:

$$k_p^u = 0.12, \quad k_p^w = 0.18, \quad k_p^\theta = 0.21, \tag{4.26}$$

$$A_p^u \sim A_p^w = 1.35, \quad A_p^\theta = 1.85, \tag{4.27}$$

respectively. It can readily be seen that the spectral bump of the passive scalar is the largest, and that of the velocity is lowest, while that of the passive vector lies between. Thus, the bottleneck effect is strongest for the passive scalar, weakest for the velocity, and intermediate for the passive vector.

Donzis and Sreenivasan[45] showed that the spectral bump decreases with increasing Reynolds number, and suggested nonlocalness in the spectral transfer as a possible mechanism for generating the spectral bump. The spectral bump has been explained as a manifestation of the bottleneck effect.[56] When one or two components in the triad interaction are only weaky excited due to the dissipation, the spectral transfer becomes less efficient, so the spectrum piles up at wave numbers just below the dissipation range. If the spectral transfer is dominated by nonlocal interactions, the lack of excitation of one or two components at distant wave numbers would result in a larger pile up of spectral excitation before the

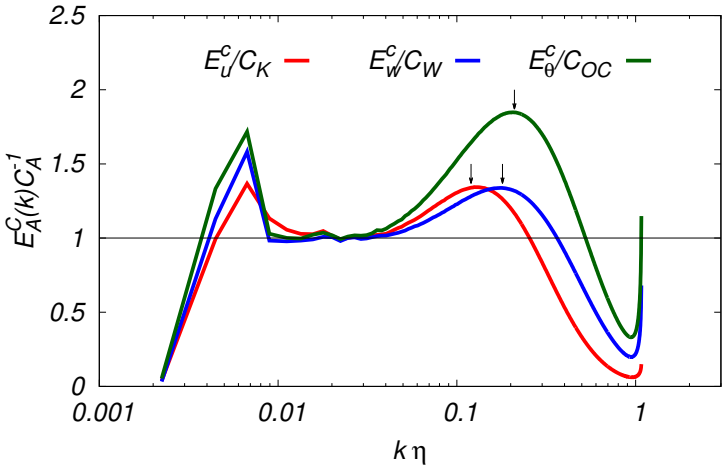

Figure 4.16: Measurement of the bottleneck effect for Run B The downwards arrows point to the peak of the compensated energy spectrum.

beginning of the spectrum roll off that occurs in the dissipation range. In other words, the stronger the nonlocalness, the larger the spectral bump appears.

To determine whether this is the case, it is studied the nonlocalness of the spectral transfer of the scalar variance by comparing it to that of the kinetic energy and passive vector variance. Using the Lagrangian renormalized approximation (LRA),[57,58,59] Gotoh and Watanabe[60] showed that in the inertial range at very high Reynolds numbers,

$$W_u(\xi) \sim C_K^2 I_u \xi^{-4/3}(\frac{4}{9}\ln\,\xi + \frac{16}{45}), \tag{4.28}$$

$$W_\theta(\xi) \sim C_K C_{OC} I_\theta \xi^{-4/3}(\frac{4}{3}\ln\,\xi + \frac{22}{45}\xi^{-4/3}), \tag{4.29}$$

$$I_u = 0.7896, \qquad I_\theta = 1.202, \tag{4.30}$$

where $\xi = \max(\mathrm{k},\mathrm{p},\mathrm{q})/\min(\mathrm{k},\mathrm{p},\mathrm{q})$ denotes the nonlocalness metric in the triad interaction, and W_A ($A = u, \theta$) represent the fractional contributions to the total mean transfer flux from the interactions in the range $[\xi, \xi + d\xi]$, defined as

$$\frac{\Pi_A}{\bar{\epsilon}_A} = \int_1^\infty W_A(\xi, k)\frac{d\xi}{\xi}. \tag{4.31}$$

They found that W_θ decays more slowly than W_u for large ξ, which means that the energy transfer of the passive scalar is less local than that of velocity field, and leads to the stronger bottleneck effect of variance of the passive scalar.

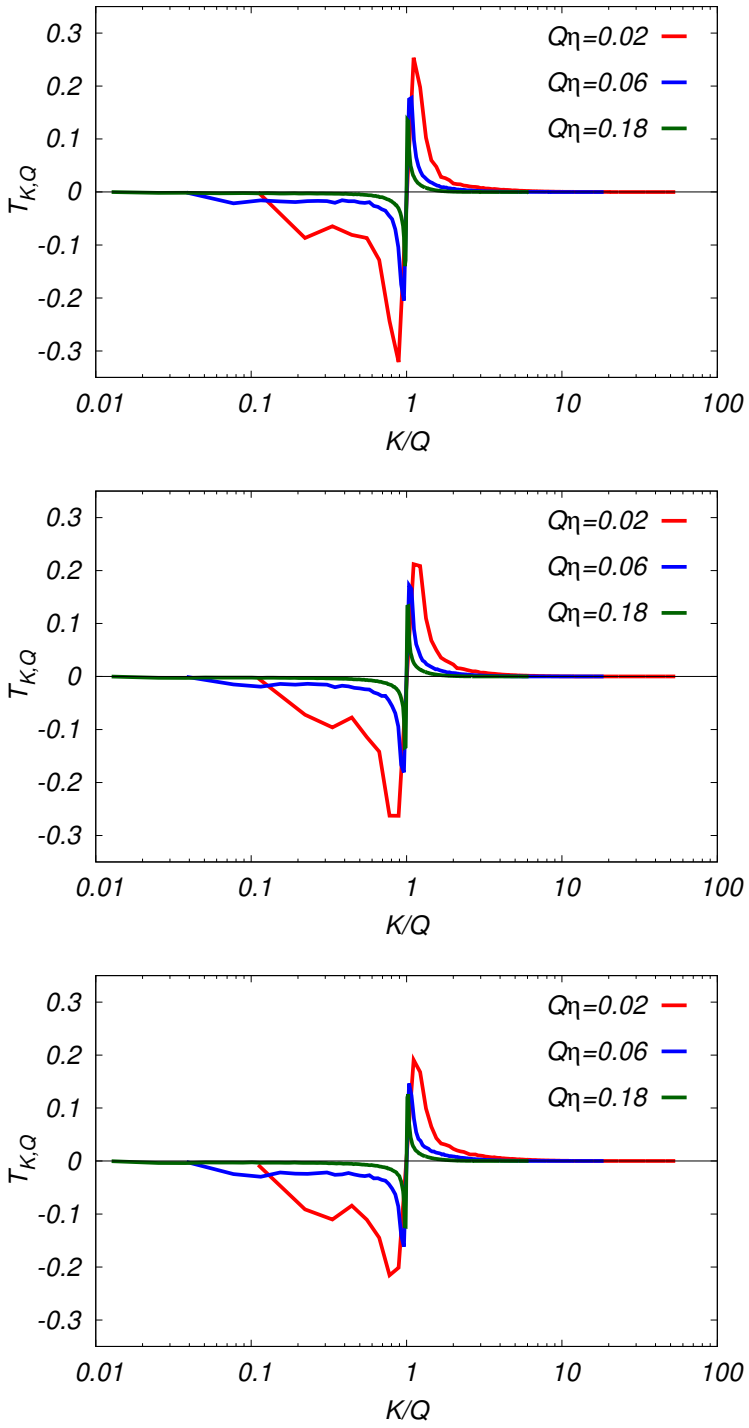

Figure 4.17: Band-to-Band transfer for Run B. Top: for kinetic energy; middle: for pseudo-kinetic energy; bottom: for passive scalar variance.

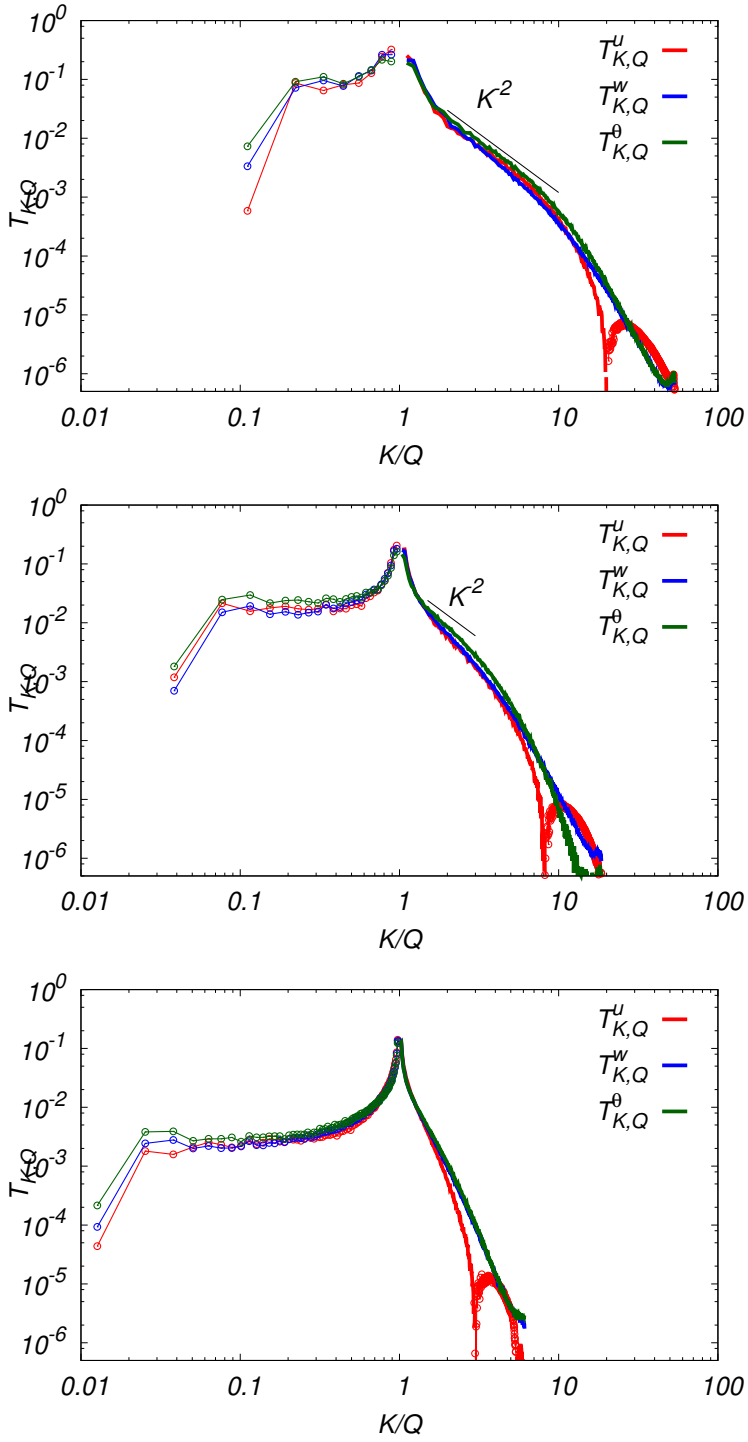

Figure 4.18: Comparison of abstract value of band-to-band transfer in logarithm scale for Run B, line with cycles denotes bands that $\mathcal{T} < 0$. Top: $Q\eta = 0.02$ as low wavenumbers; middle: $Q\eta = 0.06$ as intermediate wavenumbers; bottom: $Q\eta = 0.18$ as high wavenumbers.

Since the above results are for an infinite Reynolds number and within the LRA, we examine the cases of finite Reynolds number by using DNS. A sharp band filter G for quantity $A(\boldsymbol{x}, t)$ at band K is defined as

$$A_K(\boldsymbol{x}, t) = \mathcal{F}^{-1}\left[A(\boldsymbol{k}, t) G_K(\boldsymbol{k})\right], \tag{4.32}$$

$$G_K(\boldsymbol{k}) = \begin{cases} 1, & if \quad K - 0.5 \leq |\boldsymbol{k}| < K + 0.5, \\ 0, & otherwise. \end{cases} . \tag{4.33}$$

Then, the spectral transfer functions between band K and Q are defined in the same form as in:[61]

$$\mathcal{T}^u_{K,Q} = -\frac{1}{\overline{\epsilon}_u} \int \boldsymbol{u}_K \cdot \left[(\boldsymbol{u} \cdot \nabla)\boldsymbol{u}_Q\right] d\boldsymbol{x}, \tag{4.34}$$

$$\mathcal{T}^w_{K,Q} = -\frac{1}{\overline{\epsilon}_w} \int \boldsymbol{w}_K \cdot \left[(\boldsymbol{u} \cdot \nabla)\boldsymbol{w}_Q\right] d\boldsymbol{x}, \tag{4.35}$$

$$\mathcal{T}^\theta_{K,Q} = -\frac{1}{\overline{\epsilon}_\theta} \int \theta_K \left[(\boldsymbol{u} \cdot \nabla)\theta_Q\right] d\boldsymbol{x}, \tag{4.36}$$

respectively. $\mathcal{T}^A_{K,Q}$ represents the amount of the energy (variance) in the band Q that is transferred to the band K under the action of the turbulent velocity $\boldsymbol{u}$.

Results for Run B are shown in Fig. 4.17 and their absolute values in the logarithm scale are in Fig. 4.18. Three common features are observed:

1. $\mathcal{T}^{u,w,\theta}_{K,Q}$ are mainly negative for $K/Q < 1$, and positive for $K/Q > 1$, meaning that the energy transfer is forward cascaded,

2. the absolute value of $\mathcal{T}^{u,w,\theta}_{K,Q}$ attains the local maximum at $K/Q \sim 1$, meaning that local transfers are dominant,

3. the ratio of the local transfer to nonlocal ones decreases with increasing Q.

These results agree with previous studies.[61,62]

To study the nonlocal transfers, the plot in the logarithm scales in Fig. 4.18 is easier for visibility. It can be seen that the degree of the nonlocal transfer for $K \ll Q$ or $K \gg Q$ is in the order of $|\mathcal{T}^\theta_{K,Q}| > |\mathcal{T}^w_{K,Q}| > |\mathcal{T}^u_{K,Q}|$ for investigated Q in the present study. For small band $Q\eta = 0.02$ and intermediate band $Q\eta = 0.06$ Q, the right tails show a power law as $|\mathcal{T}^\theta_{K,Q}| \sim K^{-2}$. At near dissipative scales ($k/Q \geq 16$ and $K\eta \sim 0.4$), the transfer of the kinetic energy $\mathcal{T}^u_{K,Q}$ turns to

be negative, which is significantly different from the cases of passive vector and passive scalar. To authors' best knowledge, no explanation for this negative transfer has been found. The fact that the nonlocal transfer to small scales is most intense for the passive scalar and most mild for the velocity, is consistent with the trend for the strength of bottleneck effect on the energy spectral bump. It needs more work to clarify whether the nonlocal transfer is the reason for the bottleneck effects.

4.2.7 Discussion

The observation for low order statistics can be summarized as follows:

1. Energy spectra of $E_u(k)$, $E_w(k)$ and $E_\theta(k)$ show the Kolmogorov-Obukhov-Corrsin power law in the inertial-convective range, and the decay at dissipative range of the passive scalar and the passive vector are slower than that of the velocity, in other words, $E_w(k)$ and $E_\theta(k)$ are excited at high wave numbers when compared to $E_u(k)$. The Kolmogorov-Obukhov-Corrsin constants are $C_K(=1.57) > C_{PV}(=1.00) > C_{OC}(=0.67)$, meaning that the spectral transfer efficiency of the passive scalar is highest, and lowest for the velocity, intermediate for the passive vector.

2. As for the strength of the bottleneck effects, the passive scalar has the largest bump, the velocity has the smallest, and that of the passive vector in between. The wave number and amplitude for the peak of the bumps are in the order $k_p^u < k_p^w < k_p^\theta$ and $A_p^u \sim A_p^w < A_p^\theta$.

3. the spectra of transfer fluxes $\Pi_u(k)$, $\Pi_w(k)$ and $\Pi_\theta(k)$, show plateaus in the inertial-convective range, and decay to zero at low and high wavenumbers. The decays of $\Pi_w(k)$ and $\Pi_\theta(k)$ in the dissipative range are slower than $\Pi_u(k)$, similar to the behaviors of the energy spectra.

4. the spectrum of the pseudo-pressure $E_q(k)$ shows the same power law of k^{-2} as that of pressure $E_p(k)$, and the magnitude of $E_q(k)$ in the inertial-convective range is around $1/5 \sim 1/4$ of $E_p(k)$ at the same wave numbers.

5. the cubic moment $\langle \delta_r u_L (\delta \boldsymbol{w})^2 \rangle = -\frac{4}{3}\overline{\epsilon}_w r$ in the inertial-convective range is analytically obtained, and it has been checked numerically. It is found that the plateau value of $-\langle \delta_r u_L (\delta \boldsymbol{w})^2 \rangle / (\overline{\epsilon}_w r)$ is close to but smaller than the theoritical value 4/3 which is also similar to that of $\langle (\delta_r u_L)^3 \rangle$ and $\langle \delta_r u_L (\delta_r \theta)^2 \rangle$. Again, the similarity between the curves for the passive scalar and the passive vector in the dissipative range is observed.

From observations described above, it is concluded that for the Reynolds numbers investigated in the present study, the behavior of $\boldsymbol{w}$ resembles θ at small scales, and that the energy transfer efficiency of $\boldsymbol{w}$ is intermediate between $\boldsymbol{u}$ and θ. As seen in the visualization Section 4.1, the spatial structure of the passive vector is sheet-like which is similar to that of the passive scalar, and different from the tube-like structure of velocity. As these structures are of the length scale $[\eta, \lambda]$, the above observation is consistent with the properties found in comparison of the energy spectra, the spectra of the transfer fluxes, the 3rd order structure functions at small scales.

The pressure determined by $p(\boldsymbol{x}, t) = -\nabla^{-2}(\nabla \boldsymbol{u} : \nabla \boldsymbol{u}^T)$ and the pseudo-pressure by $q(\boldsymbol{x}, t) = -\nabla^{-2}(\nabla \boldsymbol{u} : \nabla \boldsymbol{w}^T)$ are considered as the nonlocal quantities via the Poisson kernel. The difference between p and q arises from the difference between the source terms $S_p = \nabla \boldsymbol{u} : (\nabla \boldsymbol{u})^T$ and $S_q = \nabla \boldsymbol{u} : (\nabla \boldsymbol{w})^T$. On the amplitudes, roughly speaking $|S_p| > |S_q|$ at all scales but when integrated them over the domain with the Poisson kernel weight, the difference at large scale between p and q is negligible except the amplitudes which can be absorbed into the uniform background that does not contribute their gradient ∇p and ∇q. The differences in the spatial structure between $S_p(\boldsymbol{x}, t)$ and $S_q(\boldsymbol{x}, t)$ could emerge at small scales.

On the bottleneck effects near the dissipative ranges, it is checked the scenario suggested by Falkovich that the nonlocal transfers cause the bump of the energy spectra via band-to-band transfers. It is found that the strength of the nonlocal transfer of the passive scalar is strongest, with $1.5 \sim 2$ times of that of the velocity, and that of passive vector is in between the passive scalar and the velocity. The trend is consistent with that the strength of bottleneck effect is in the order of

$A_p^u \sim A_p^w (= 1.2) < A_p^\theta (= 1.9)$, although it is necessary to check the relation between the nonlocal transfers and the bottleneck effect deeper.

It is useful to recall the behavior of turbulence in $\mathcal{D}$ dimensions.[63] When the spatial dimension $\mathcal{D}$ increases, the incompressibilty constraint weakens, because the number of terms such that $\partial u_i/\partial x_i = 0$ increases with $\mathcal{D}$, thus dimishing the contributions of the pressure. In this case, the relative importance of the convective action increases, meaning that the nonlinearity dominates the small scale dynamics. One implication of this arguement is that the incompressibilty condition for the passive vector, which is assured by the pseudo-pressure, is of secondary importance to the small scale dynamics of the passive vector, and the convective term is a main player. Therefore, whether the convective term is linear or nonlinear make differences at small scales, while the pseudo-pressure becomes appreciable for large-scale statistics.

4.3 High Order Statistics

4.3.1 One Point Probability Density Functions

Normalized one point probability density functions (PDFs) of one component of vectors and scalar for Run B and E are shown in Fig. 4.19. Slight asymmetry of PDFs is observed and we consider it is due to the finite length of the time average and the forcing at low wave number band. Since Run E is forced at high wave number band, which means that the number of forcing Fourier mode is much larger than that of Run B, so that the better statistical convergence is expected. Indeed, the asymmetry of $P(u_1)$, $P(w_1)$ and $P(\theta)$ is weaker than Run B. The curve of $P(u_1)$ is close to Gaussian distribution and $P(\theta)$ decays faster, which is consistent with the observation in Refs.[15,24,49] There are studies reporting that $P(\theta)$ is Gaussian, exponential, or stretched exponential,[64,65,66,67] depending on conditions. It is also noted that $P(w_1)$ is wider than Gaussian at large amplitude. It is not known how this trend is caused, which is one of subjects in the future study.

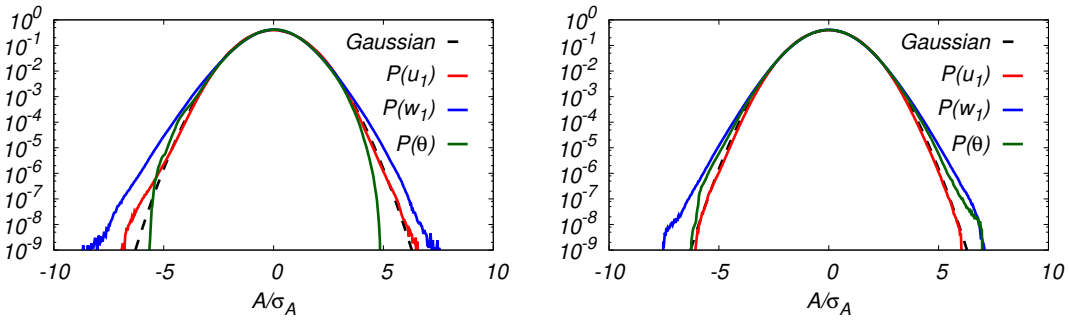

Figure 4.19: Normalized probability density functions of u_1, w_1 and θ. $A = u_1, w_1, \theta$, and σ_A denotes the standard deviation. Left: for Run B ($R_\lambda \sim 300$, low-k forcing); Right: for Run E ($R_\lambda \sim 90$, high-k forcing).

The normalized PDF of the pressure and the pseudo-pressure for Run B and Run E are shown in Fig. 4.20. $P(p)$ is negatively skewed and has a long left tail, consistent with previous studies.[68,69] The left tail of $P(q)$ for Run B is slightly longer than the right tail but symmetry is stronger than that of $P(p)$. It is not known whether the asymmetry of $P(q)$ remains finite or vanishes when the time average is extened or whether it depends on the method of external injection. But it can be observed that $P(q)$ for Run E is more symmetric than Run B.

As discussed in Section 4.1.1, there are strong vortex tubes in turbulences. For fluid particles to rotate around the centeral line of the thin vortex cube, the pressure inside the tube must be much lower than outside pressure. Therefore, the long left negative tail of $P(p)$ prevails. On the other hand, the structure of Ω_θ is sheet-like, so as that of Ω_w for the passive vector . For the sheet-like structure, a volume adjoined to one side of the surface almost equals to the volume adjoined to the opposite side, and the sheet could be formed by the difference in δq between the both sides irrespective of sign of δq, so that the distribution of pseudo-pressure is more symmetric than pressure.

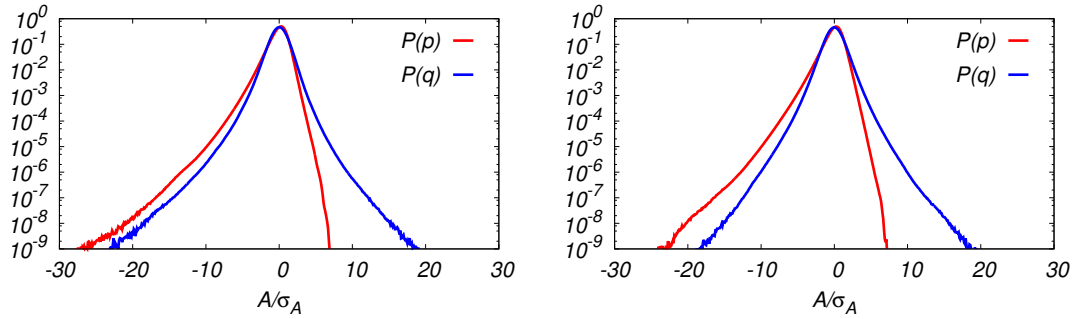

Figure 4.20: Normalized probability density functions of p and q. $A = p, q$, and σ_A denotes the standard deviation. Left: for Run B ($R_\lambda \sim 300$, low-k forcing); right: for Run E ($R_\lambda \sim 90$, high-k forcing).

4.3.2 Probability Density Functions of Derivatives

The PDFs of the fields gradient for Run A are shown in Fig. 4.21. The observations are as follows: (1) $P(\partial u_1/\partial x_1)$ is negatively skewed which is linked to the energy transfer from larger scales to smaller scales.[49] On the other hand, $P(\partial w_1/\partial x_1)$ is symmetric and has a long tail than that of $P(\partial u_1/\partial x_1)$. (2) the PDFs of the transverse gradient of the velocity and the passive vector are symmetric, and wider than that of the longitudinal gradient. The PDFs of the gradient of the passive scalar $P(\partial\theta/\partial x_1)$ is widest and has longest tails. The normalized PDF of the gradients of the pressure $P(\partial p/\partial x_1)$ and the pseudo-pressure $P(\partial q/\partial x_1)$ for Run A are shown in Fig. 4.22. The PDFs are symmetric and almost collapse onto each other.[69,70]

4.3.3 Probability Density Functions of Energy Dissipative Rate and Enstropy

The PDFs of $\log_{10}(\epsilon_\mathrm{A}/\overline{\epsilon}_\mathrm{A})$ are shown in top panel of Fig. 4.23, where the energy dissipation rate for $\boldsymbol{u}$, $\boldsymbol{w}$, θ here are computed as

$$\epsilon_u = \nu(\nabla \boldsymbol{u})^2, \tag{4.37}$$

$$\epsilon_w = \alpha(\nabla \boldsymbol{w})^2, \tag{4.38}$$

$$\epsilon_\theta = \kappa(\nabla \theta)^2, \tag{4.39}$$

respectively.

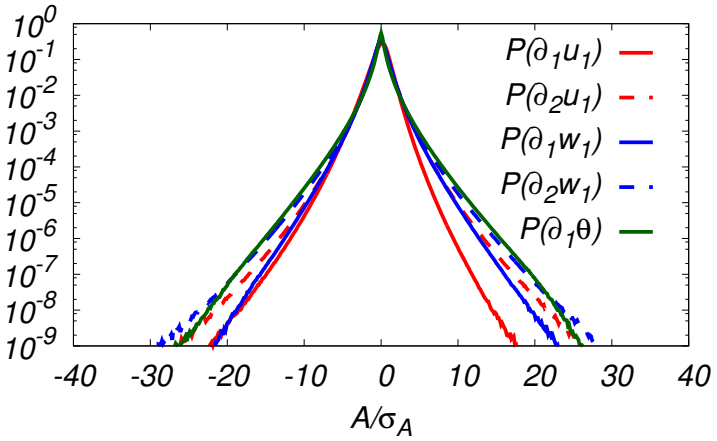

Figure 4.21: Normalized probability density functions of $\partial u_1/\partial x_1$, $\partial u_1/\partial x_2$, $\partial w_1/\partial x_1$, $\partial w_1/\partial x_2$ and $\partial \theta/\partial x_1$ for Run A.

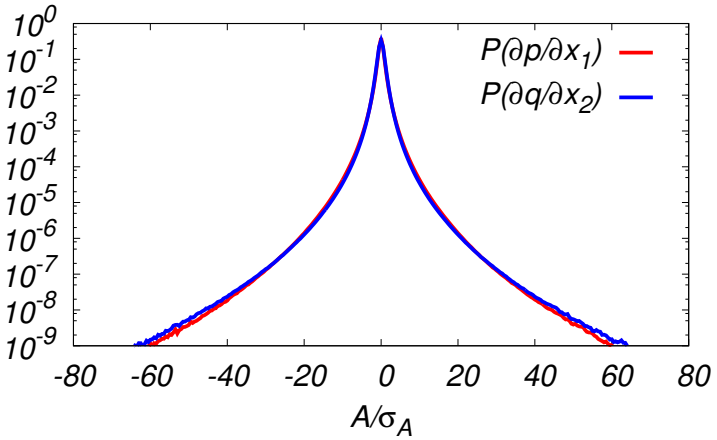

Figure 4.22: Normalized probability density functions of $\partial p/\partial x_1$ and $\partial q/\partial x_1$ for Run A.

The right tail of PDFs of $\log_{10}(\epsilon_\mathrm{u}/\overline{\epsilon}_\mathrm{u})$ and $\log_{10}(\epsilon_\mathrm{w}/\overline{\epsilon}_\mathrm{w})$ collapse very well and close to the log-normal distribution.[38] In the case of incompressible HIT turbulence, energy dissipation rate for $\boldsymbol{u}$, $\boldsymbol{w}$ can also be represented by

$$\epsilon_u^* = 2\nu(S_{ij}^u)^2, \tag{4.40}$$

$$\epsilon_w^* = 2\alpha(S_{ij}^w)^2, \tag{4.41}$$

respectively, and it is defined as $\beta^* = \log_{10}(\epsilon_\mathrm{A}^*/\overline{\epsilon}_\mathrm{A}^*)$, and shown in bottom panel

of Fig. 4.23.

On the other hand, the left tail of PDF decays linearly with slope $n_\theta = 3/2$, $n_{u,w} = 4$, $n^*_{u,w} = 5/2$, which means that

$$P(\ln\epsilon_A)d\ \ln\epsilon_A \propto \exp(n_A|\ln(\epsilon_A/\overline{\epsilon}_A)|)\mathrm{d}\ \ln\epsilon_A \propto (\epsilon_A)^{n_A-1}\mathrm{d}\epsilon_A,$$

so that

$$P(\epsilon_u) \propto \epsilon_u^3, \tag{4.42}$$

$$P(\epsilon_w) \propto \epsilon_w^3, \tag{4.43}$$

$$P(\epsilon_u^*) \propto \epsilon_u^{*\,3/2}, \tag{4.44}$$

$$P(\epsilon_w^*) \propto \epsilon_w^{*\,3/2}, \tag{4.45}$$

$$P(\epsilon_\theta) \propto \epsilon_\theta^{1/2}, \tag{4.46}$$

for small ϵ_θ.

P. K. Yeung studied the PDFs for $x = \epsilon/(\nu\Omega)$, the ratio of the kinetic energy dissipation rate to the enstropy, and found that the PDF tails obey the power law as $P(x) \propto x^{3/2}$ and $x^{-5/2}$ for small and large x, respectively. The enssence of the argument is that the weak dissipation or weak enstropy corresponds to the nearly Gaussian velocity field and obeys the chi-square distribution,

$$\chi_k(z) = \frac{1}{\Gamma(k/2)} z^{k/2-1} e^{-z/2}, \tag{4.47}$$

with the degree of freedom k, where Γ is the Gamma function.

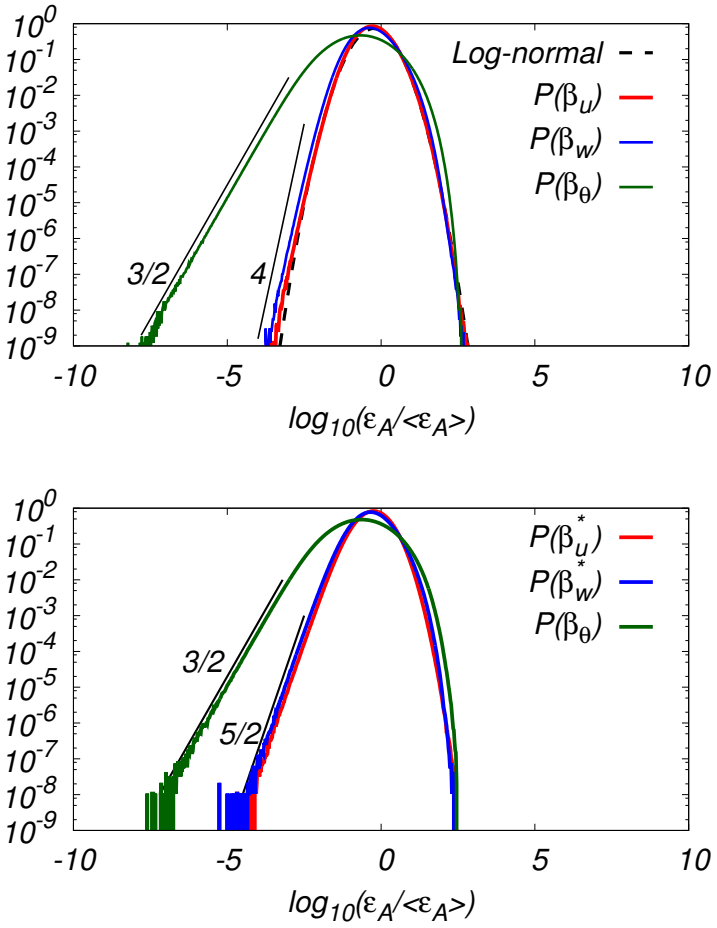

Figure 4.23: Probability density functions of $\beta_A = \log_{10}(\epsilon_\mathrm{A}/\overline{\epsilon}_\mathrm{A})$ (A denotes u, w or θ) for Run A. Top panel: energy dissipation rates caculated by $\epsilon_A = \nu_A(\nabla A)^2$; bottom panel: energy dissipation rates caculated by $\epsilon'_A = 2\nu_A\left(S^A_{ij}\right)^2$.

If the same argument is applied to the scalar destruction rate ϵ_θ, we obtain $\chi_3(\epsilon_\theta) \propto \epsilon_\theta^{1/2}$ with $k = 3$, because ϵ_θ is the sum of the three squared terms, which agrees well with Eq. (4.46). Under the incompressibility constraints, $\epsilon_u = \nu(\partial_i u_j)^2$ has freedom degree of eight, because $\partial u_3/\partial x_3 = -\partial u_2/\partial x_2 - \partial u_1/\partial x_1$, and $\chi_8(\epsilon_u) \propto \epsilon_u^4$ agrees with Eq. (4.42), so as to distribution of ϵ_w for small values.

Moreover, $\epsilon^*_u = (\nu/2)(\partial_i u_j + \partial_j u_i)^2$ has freedom degree of five $(S_{11}, S_{22}, S_{12}, S_{23}, S_{31})$, because that

$$S_{21} = S_{12}, \qquad S_{13} = S_{31}, \qquad S_{32} = S_{23}, \qquad S_{33} = -S_{11} - S_{22},$$

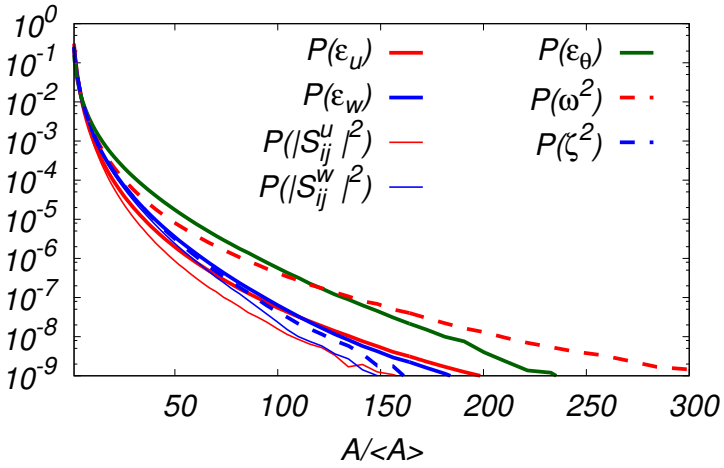

Figure 4.24: Probability density functions of ϵ_u, ϵ_w, $|S^u_{ij}|^2$, $|S^w_{ij}|^2$, and ϵ_θ for Run A.

and $\chi_5(\epsilon^*_u) \propto \epsilon^{*3/2}_u$ agrees with Eq. (4.44), so as to distribution of ϵ^*_w for small values. This suggests that for weak amplititudes of the dissipations, the statistics Eq. (4.47) dominates the dynamics.

The PDFs normalized by the average value of energy dissipation rate $P(\epsilon_u/\overline{\epsilon}_u)$, $P(\epsilon_w/\overline{\epsilon}_w)$, $P(\epsilon_\theta/\overline{\epsilon}_\theta)$ and enstropy $P(\boldsymbol{\omega}^2/\overline{\boldsymbol{\omega}^2})$, $P(\boldsymbol{\zeta}^2/\overline{\boldsymbol{\zeta}^2})$ are shown in Fig. 4.24. The PDF tail of $P(\boldsymbol{\omega^2})$ is longer than that of $P(\epsilon_u)$, which is consistent with result of Ref,[71] on the other hand, the PDF tails of $P(\boldsymbol{\zeta}^2)$ and $P(\epsilon_w)$ are close to each other.

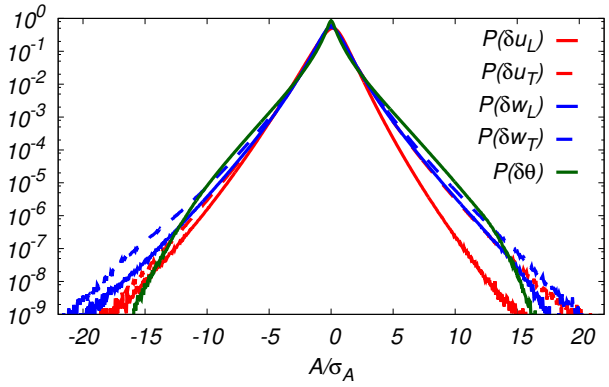

(a)

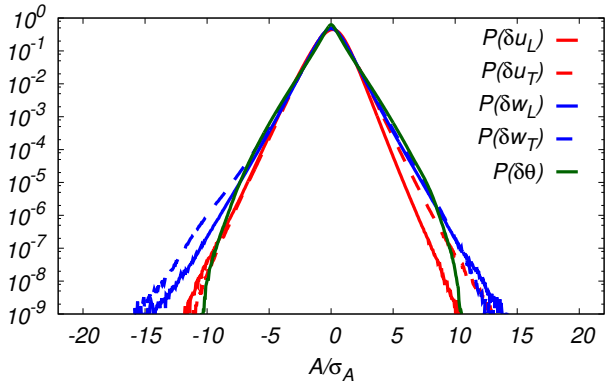

(b)

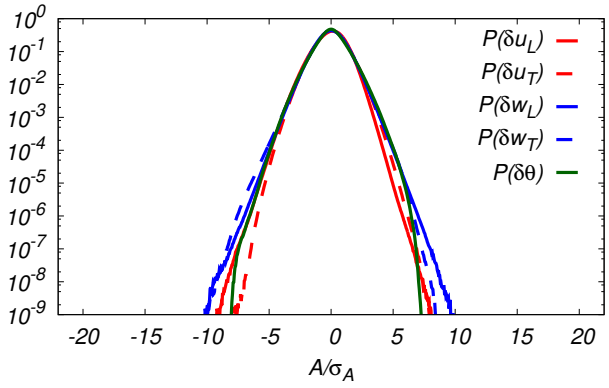

(c)

Figure 4.25: Probability density functions of increments for Run B. (a), (b), (c): PDF of δu_L, δu_T, δw_L, δw_T and $\delta\theta$ with r of $4\Delta x$, $16\Delta x$, $64\Delta x$ respectively

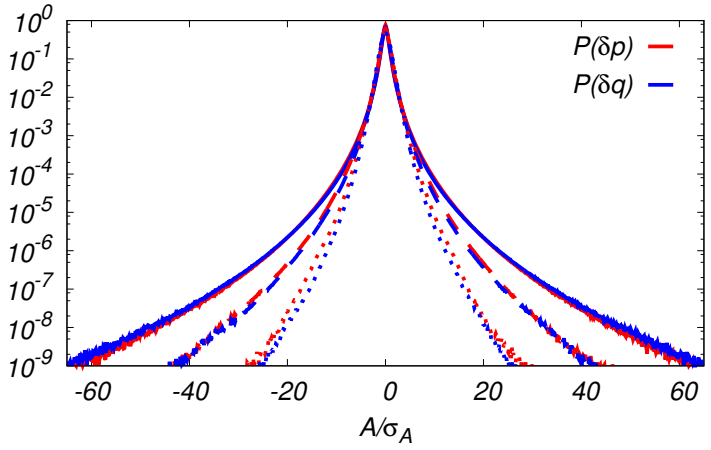

Figure 4.26: PDF of δp and PDF of δq.

4.3.4 Two Points Probability Density Functions

Increment of field at two points separated by the distance r is written as

$$\delta_r A_B = [\boldsymbol{A}(\boldsymbol{x}+\boldsymbol{r}) - \boldsymbol{A}(\boldsymbol{x})] \cdot \boldsymbol{e}_B \tag{4.48}$$

for vector where A denotes u or w and B stands for the longitudinal (L) or transverse(T) component to the direction of $\boldsymbol{r}$, and

$$\delta_r C = C(\boldsymbol{x}+\boldsymbol{r}) - C(\boldsymbol{x}) \tag{4.49}$$

for scalars where C stands for θ, p or q. $P(\delta u_L, r)$, $P(\delta u_T, r)$, $P(\delta w_L, r)$, $P(\delta w_T, r)$, $P(\delta\theta, r)$ and $P(\delta p, r)$, $P(\delta q, r)$ with $r = (4, 16, 64)\Delta$x for Run B are shown in Fig. 4.25, Fig. 4.26, respectively. The PDFs become narrow as the separation distance increases, and their tails change from concave to convex, which are consistent with Refs.[49,15] The PDF tails at large amplitudes as a measure of the wideness of the PDF are in the order of $P(\delta u_L, r)$, $P(\delta w_L, r)$, and $P(\delta u_T, r) \sim P(\delta w_T, r)$ for all separation distance studied. $P(\delta u_L, r)$ is also negatively skewed like behavior in Fig. 4.21. $P(\delta p, r)$ and $P(\delta q, r)$ are symmetric and close to each other at a small separation distance, but $P(\delta q, r)$ become slightly narrower than $P(\delta p, r)$ when separation distance increases.

4.3.5 Scaling Exponents of Field Increment Moments

It is expected the moments of the increment of fields in turbulence obey a power law in the inertial-convective range, which are defined as

$$S_p^{uL}(r) = \langle |\delta_r u_L|^p \rangle \propto r^{\xi_p^{uL}}, \tag{4.50}$$

$$S_p^{uT}(r) = \langle |\delta_r u_T|^p \rangle \propto r^{\xi_p^{uT}}, \tag{4.51}$$

$$S_p^{wL}(r) = \langle |\delta_r w_L|^p \rangle \propto r^{\xi_p^{wL}}, \tag{4.52}$$

$$S_p^{wT}(r) = \langle |\delta_r w_T|^p \rangle \propto r^{\xi_p^{wT}}, \tag{4.53}$$

$$S_p^{\theta}(r) = \langle |\delta_r \theta|^p \rangle \propto r^{\xi_p^{\theta}}, \tag{4.54}$$

respectively.

To evaluate how the scaling behavior varies with respect to the separation distance r, following functions of r are examined first,

$$\xi_p^A(r) = \frac{d \ln S_p^A(r)}{d \ln r}, \tag{4.55}$$

A denotes for uL, uT, wL, wT, or θ and results for Run C are shown in Fig. 4.27. Since the most of interest is in the scaling behavior in the inertial-convective range at high Reynolds number which is expected to be insensitive to the dissipation range,[42] the curves of the local scaling exponents for Run C which has the highest Reynolds number and the broadest inertial-convective range in present study are chosen to examine.

The observation is as follows:

1. General trend of the curves is that when r/η increases from the dissipation range, the curves decrease from value close to the analytical value p for p-th order moments, then become nearly horizontal at around $r/\eta \sim 100$ where the power law scaling is expected, and finally decay at large separation distances.

2. The width of horizontal range becomes wider approximately in the order of $\delta_r u_L$, $\delta_r u_T$, $\delta_r w_L$ and $\delta_r w_T$.

3. On the low end of the horizontal part of the curve $r_{*,p}^{A,B}$ where A is u, w and B is L and T, it is found that $r_{*,p}^{A,T} < r_{*,p}^{A,L}$, (consistent with Ref.[49] for $A = u$), and that $r_{*,p}^{w,B} < r_{*,p}^{u,B}$ both $B = L$ and T.

4. The curves of the local scaling exponents of $\xi_p^\theta(r)$ do not have a plateau but have local minimum values at $r/\eta \sim 60$, linearly increase with r in the range $70 < r/\eta < 300$, and arrive at local maximum values at $r/\eta \sim 600$, which are consistent with Refs.[15,27]

5. the local scaling exponents ξ_p^{wL} and ξ_p^{wT} show similar behavior to ξ_p^θ that linearly increase when $p = 8$, which suggests that the scaling exponents of the passive vector are not universal as predicted in Refs.[31,33]

Since the Reynolds numbers in present DNS runs are not high enough and the plateau width of the curves are still short, it is difficult to determine the scaling exponents in the inertial-convective range. In present study, the ranges where the scaling exponents are computed are determined by the following method. It is considered,

$$\varphi^A(r^*) = \frac{d\ \xi_4^A(r)}{d\ \ln\ r^*}, \tag{4.56}$$

where $r^* = r/\eta$, and choose the range that $|\varphi^A| < 0.3$ for ξ_p^{uL}, $|\varphi^A| < 0.1$ for ξ_p^{uT}, ξ_p^{wL}, ξ_p^{wT}, $\varphi^A > 0$ for ξ_θ by considering the fact that the peak of $\varphi^{uL}(r^*)$ is much smaller than others, $\varphi^\theta(r^*)$ has the widest range of positive values and the highest peak. Within this range, the mean value $\overline{\xi}_p^A$, the minimum value $\xi_{p,min}^A$ and the maximum value $\xi_{p,max}^A$ are calculated. The results for Run C are shown in top panel Fig. 4.29 with error bars which are computed as the deviation of the minimum and maximum values from the mean. It is found that $\xi_p^\theta < \xi_p^{wT} < \xi_p^{wL} < \xi_p^{uT} < \xi_p^{uL} < p/3$ when $p > 4$, which means that the intermittency of the passive vector lies between the velocity field and the passive scalar, and the scaling of the passive vector is anomalous.

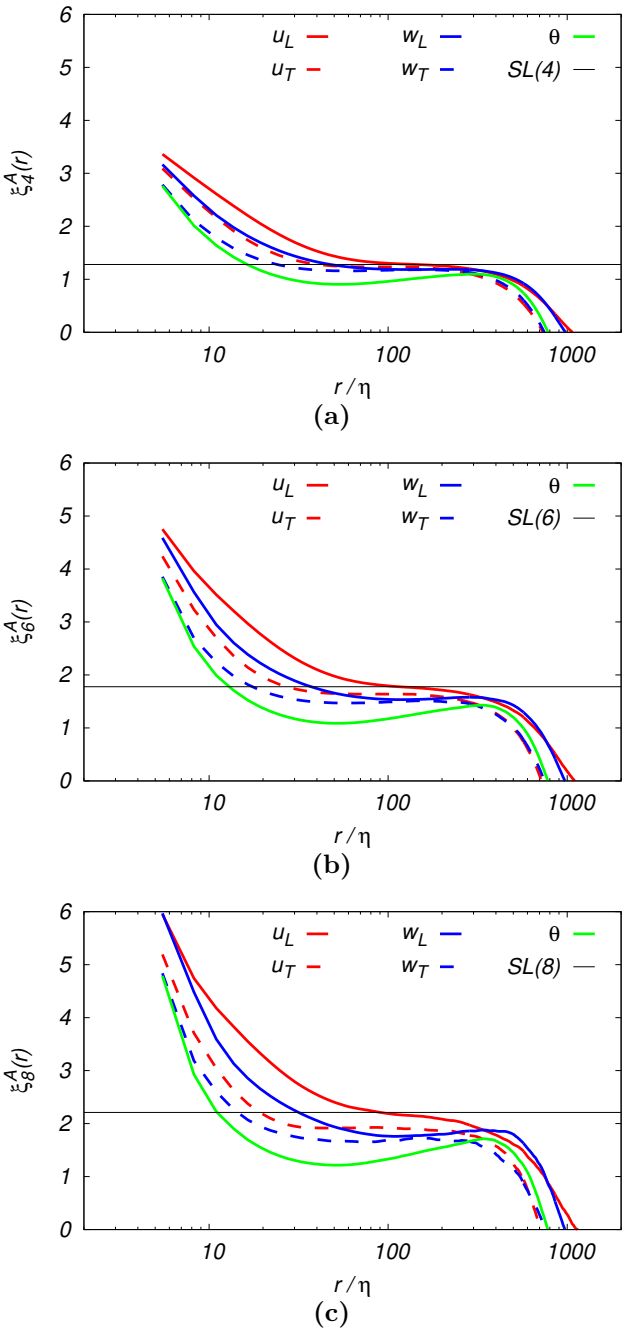

Figure 4.27: Scaling exponents of moments of fields increment for Run C. (a), (b), (c): $\xi_p^{uL}(r\eta^{-1})$, $\xi_p^{uT}(r\eta^{-1})$, $\xi_p^{wL}(r\eta^{-1})$, $\xi_p^{wT}(r\eta^{-1})$ and $\xi_p^{\theta}(r\eta^{-1})$ with p of 4, 6 and 8 respectively.

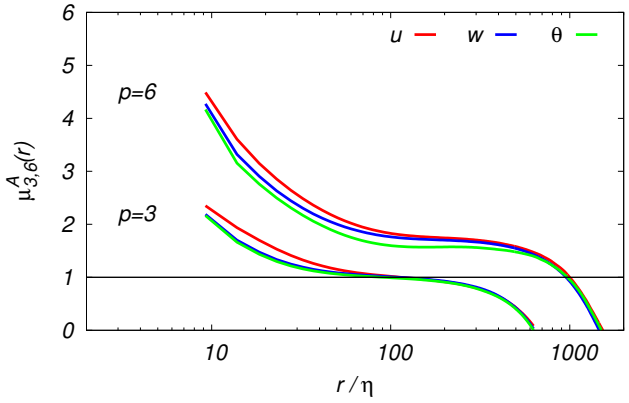

Figure 4.28: Scaling exponents of fluxes for Run C for $p = 3, 6$.

4.3.6 Scaling Exponents of Energy Flux Moments

The transfer fluxes of the kinetic energy, the pseudo-kinetic energy and the variance of passive scalar as functions of the separation distance Δ, are defined in terms of the product of the filterized rate of strain tensor, the Reynolds stress with filter width Δ, but it requires a large number of computations. To avoid this, in this study the moments of 3rd order structure functions as surrogates of the transfer fluxes is used and defined as

$$Q_p^u(r) = r^{p/3}\Pi_{p/3}^u(r) = -\left\langle \left[\delta_r u_L(\delta_r \boldsymbol{u})^2\right]^{p/3} \right\rangle \propto r^{\mu_p^u}, \tag{4.57}$$

$$Q_p^w(r) = r^{p/3}\Pi_{p/3}^w(r) = -\left\langle \left[\delta_r u_L(\delta_r \boldsymbol{w})^2\right]^{p/3} \right\rangle \propto r^{\mu_p^w}, \tag{4.58}$$

$$Q_p^\theta(r) = r^{p/3}\Pi_{p/3}^\theta(r) = -\left\langle \left[\delta_r u_L(\delta_r \theta)^2\right]^{p/3} \right\rangle \propto r^{\mu_p^\theta}, \tag{4.59}$$

respectively. As far as the scaling arguments are concerned, the above moments are expected to provide equivalent knowledge of the scaling behavior of the transfer fluxes. Similar to the processes in Section 4.3.5, we examined the local scaling exponents defined by

$$\mu_p^A(r) = \frac{d \ln Q_p^A(r)}{d \ln r}, \tag{4.60}$$

where A denotes for u, w, or θ. Results for Run C are shown in Fig. 4.28.

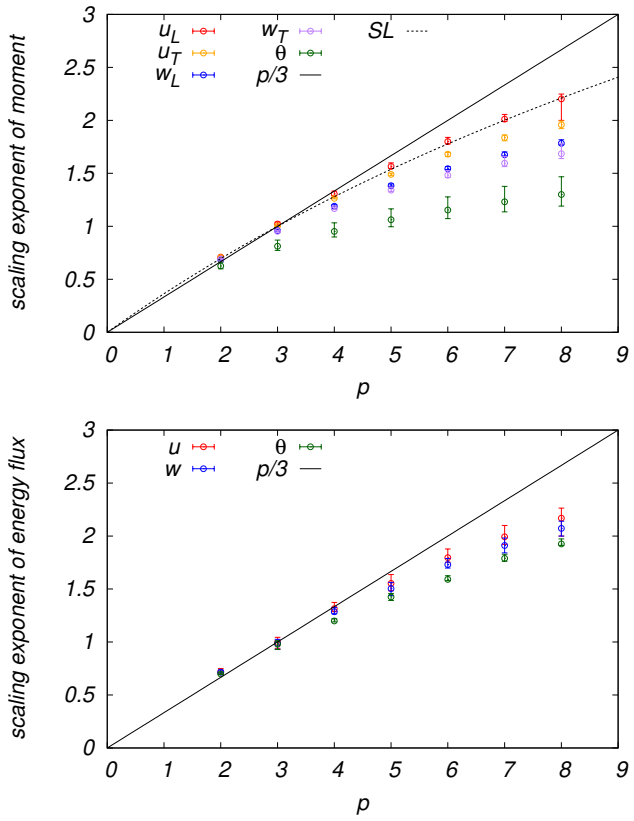

Figure 4.29: Scaling exponents of moments of increments and fluxes for Run C. Top panel: average, minimal and maximum value of ξ_p^{uL}, ξ_p^{uT}, ξ_p^{wL}, ξ_p^{wT}, and ξ_p^{θ} in the inertial range ; bottom panel: average, minimal and maximum value of μ_p^u, μ_p^w and μ_p^{θ} in the inertial range.

The observations are:

1. the range of the plateaus for $\mu_p^u(r)$, $\mu_p^w(r)$, $\mu_p^{\theta}(r)$ for fixed p is not so different as that of $\xi_p^A(r)$.

2. $\mu_p^{\theta}(r)$, $\mu_p^u(r)$ and $\mu_p^w(r)$ are close to one another.

3. the low end and high end distance of plateaus $r_{*,3}^{\mu^A}$ is smaller than those of $r_{*,6}^{\mu^A}$.

The values of the scaling exponents are determined in the same way as that for ξ_p^A. The r_{min} is chosen as r satisfied $d\mu_3^u/d\ln r^* > -0.3$, and r_{max} satisfied

$d\mu_6^u/d\ln r^* > -0.3$, the mean value $\overline{\mu}_p^A$, minimum value $\mu_{p,min}^A$ and maximum value $\mu_{p,max}^A$ are calculated and the results for Run C are shown in bottom panel of Fig. 4.29 with error bars. It is found that:

1. the amplitudes of fluctuation of μ_p^A in the inertial-convective range, $\mu_{p,max}^A - \mu_{p,min}^A$ is smaller than those of ξ_p^A when $n > 4$.

2. the offset from $n/3$ of μ_p^A for $A = w$ or θ is smaller than those of ξ_p^A when $n > 4$, and again the order is $\mu_p^\theta < \mu_p^w < \mu_p^u$ when $n > 4$, meaning that the intermittency of the passive vector transfer flux is between that of the velocity and the passive scalar.

4.3.7 Effects of Reynolds Number and Forcing Method

The effects of the Reynolds number and large-scale forcing on the scaling exponents are examined in Section 4.3.7. Run E is not included as Reynolds number is too small to find plateau ranges. The effects of Reynolds number can be checked by comparing Runs A, B and C for the same forcing method, and large-scale forcing effects can be checked by comparing Run B and D at almost same Reynolds numbers. Althogh the Reynolds numbers in the present computations are not enough to fully determined the trend, and the scaling exponents are slightly scattered, the general trend is that the scaling exponents are insensitive to the variation of the Reynolds numbers and large-scale forcing in the present study.

Table 4.1: Scaling exponents of moments of increments and transfer fluxes in the inertial range. Mean, standard deviation, maximaum and minimum values are computed in the range $[r_{\min}/\eta, r_{\max}/\eta]$ in which the absolute value of the local slope is smaller than specific values. For Run A, ξ_p^{uL} and μ_p^A are not computed because of short range.

		Run A				Run B				Run C				Run D			
	range / p	mean	std	min	max	mean	std	min	max	mean	std	min	max	mean	std	min	max
ξ_p^{uL}	range		n/a				$[80, 233]$				$[82, 310]$				$[85, 199]$		
	4					1.28	0.02	1.24	1.33	1.30	0.02	1.25	1.34	1.26	0.03	1.21	1.30
	6					1.76	0.04	1.69	1.83	1.79	0.03	1.72	1.85	1.72	0.04	1.64	1.79
	8					2.15	0.05	2.00	2.24	2.19	0.03	2.00	2.26	2.08	0.06	1.99	2.18
ξ_p^{uT}	range		$[56, 126]$				$[52, 159]$				$[55, 204]$				$[52, 120]$		
	4	1.21	0.00	1.21	1.22	1.24	0.01	1.22	1.25	1.26	0.01	1.24	1.27	1.23	0.01	1.21	1.25
	6	1.60	0.03	1.57	1.65	1.64	0.00	1.62	1.65	1.67	0.02	1.64	1.70	1.64	0.02	1.60	1.66
	8	1.88	0.07	1.79	2.01	1.92	0.01	1.89	1.93	1.95	0.03	1.91	1.99	1.91	0.03	1.86	1.94
ξ_p^{wL}	range		$[70, 146]$				$[74, 307]$				$[78, 424]$				$[80, 217]$		
	4	1.22	0.01	1.20	1.23	1.19	0.01	1.17	1.21	1.19	0.01	1.18	1.21	1.19	0.02	1.17	1.22
	6	1.60	0.00	1.60	1.61	1.55	0.02	1.53	1.58	1.55	0.01	1.54	1.58	1.57	0.02	1.53	1.61
	8	1.88	0.03	1.85	1.92	1.79	0.03	1.76	1.86	1.81	0.04	1.77	1.89	1.81	0.03	1.78	1.87
ξ_p^{wT}	range		$[36, 125]$				$[41, 239]$				$[43, 350]$				$[46, 191]$		
	4	1.20	0.01	1.19	1.21	1.17	0.01	1.16	1.18	1.17	0.01	1.16	1.19	1.14	0.01	1.12	1.16
	6	1.54	0.03	1.51	1.58	1.49	0.01	1.47	1.51	1.50	0.03	1.46	1.54	1.44	0.01	1.43	1.46
	8	1.77	0.06	1.71	1.90	1.68	0.02	1.65	1.73	1.71	0.06	1.64	1.79	1.59	0.05	1.53	1.69
ξ_p^{θ}	range		$[47, 146]$				$[54, 294]$				$[59, 412]$				$[57, 196]$		
	4	1.03	0.05	0.96	1.11	1.00	0.07	0.90	1.10	1.01	0.08	0.90	1.13	0.94	0.03	0.90	0.98
	6	1.29	0.09	1.17	1.45	1.23	0.11	1.09	1.42	1.25	0.13	1.07	1.50	1.15	0.04	1.09	1.21
	8	1.50	0.13	1.33	1.73	1.41	0.14	1.22	1.68	1.44	0.20	1.19	1.84	1.29	0.05	1.23	1.36
	range		n/a				$[52, 186]$				$[47, 275]$				$[54, 165]$		
μ_p^u	3					0.94	0.07	0.79	1.04	0.97	0.07	0.80	1.06	0.95	0.06	0.83	1.03
	6					1.77	0.04	1.70	1.86	1.79	0.06	1.72	1.93	1.75	0.05	1.67	1.85
μ_p^w	3					0.95	0.06	0.81	1.02	0.96	0.07	0.79	1.04	0.94	0.05	0.83	1.01
	6					1.72	0.03	1.66	1.79	1.72	0.04	1.66	1.83	1.72	0.04	1.66	1.79
μ_p^{θ}	3					0.93	0.06	0.78	1.00	0.95	0.06	0.79	1.02	0.94	0.05	0.83	1.00
	6					1.58	0.01	1.56	1.62	1.60	0.02	1.58	1.67	1.54	0.03	1.49	1.60

4.3.8 Discussion

The observations for the high order statistics are following:

1. $P(w_1)$ is wider than $P(u_1)$ which is approximately Gaussianly distributed, and $P(\theta)$ is convex at extreme values.

2. $P(\log_{10}(\epsilon_u/\overline{\epsilon})_u)$ and $P(\log_{10}(\epsilon_w/\overline{\epsilon})_w)$ are close to each other, $P(\epsilon_u)$ and $P(\epsilon_w)$ are approximately log-normal distributed. The right tail of $P(\ln(\epsilon_\theta/\overline{\epsilon})_\theta)$ is similar to the above two PDFs, but the left tail shows a power law slope $n_\theta \sim 3/2$ and $n_{u,w} \sim 4$, meaning that $P(\epsilon_\theta) \sim \epsilon_\theta^{1/2}$, $P(\epsilon_u) \sim \epsilon_u^3$ and $P(\epsilon_w) \sim \epsilon_w^3$ for small values.

3. $P(p)$ is clearly negatively skewed, while $P(q)$ is approximately symmetric.

4. $P(\epsilon_u)$ is longer tail than $P(\boldsymbol{\omega}^2)$, but $P(\boldsymbol{\zeta}^2)$ and $P(\epsilon_w)$ have similar tail.

5. On the local scaling exponents of increment moments, the small curves of $\xi_p^{A,B}(r)$(A is u or w, B is L or T) have plateau and $r_{*,p}^{A,T} < r_{*,p}^{A,L}$ and $r_{*,p}^{w,B} < r_{*,p}^{u,B}$, while the curve of $\xi_p^\theta(r)$ shows a linear function of $\ln(r/\eta)$. Moreover, $\xi_p^{wL}(r)$ and $\xi_p^{wT}(r)$ for $p = 8$ become to linearly increase with $\ln(r/\eta)$, meaning that the scaling exponents at high order of the passive vector increment moments are not universal.

6. The curves of $\mu_p^u(r)$, $\mu_p^w(r)$ and $\mu_p^\theta(r)$ are close to one another.

7. The scaling exponents in the inertial-convective range are in the order of $p/3 > \xi_p^{uL} > \xi_p^{uT} > \xi_p^{wL} > \xi_p^{wT} > \xi_p^\theta$ and $p/3 > \mu_p^u > \mu_p^w > \mu_p^\theta$, meaning that the passive scalar is the most intermittent, the velocity is least intermittent, and the passive vector is intermediate between them.

The PDFs of the dissipation rate of the kinetic energy and pseudo kinetic energy are close to log-normal distribution as suggested by K62. It should be noted that the scaling exponents at high order of the passive vector is non-universal and anomalous, which differs from the prediction based on the Kraichnan velocity ensemble or the numerical study by the shell models. From the arguements in the previous and the present sections, although the kinetic constraints of $\nabla \cdot \boldsymbol{w} = 0$

and the pseudo-pressure are common features with those of the Navier-Stokes velocity field, they are not enough to acheive the same degree of the intermittency behavior for $\boldsymbol{w}$ as that for $\boldsymbol{u}$. Rather the linearity of $\boldsymbol{w}$ in the convective terms tends to generate the stronger intermittency of $\boldsymbol{w}$. The solenodal condition through the pseudo-pressure tends to relax the intermittency of $\boldsymbol{w}$.

5

Summary

To explore the physical mechanism underlying the similarities and differences in the statistical properties of velocity and passive scalar fluctuations, we introduced an incompressible passive vector incorporating pseudopressure, which shares many common properties with both the Navier-Stokes and passive scalar equations. Statistical data obtained from DNSs showed that the passive vector shares common statistical properties with the velocity and passive scalars, especially for low order statistics, such as the power law of the energy spectra, the transfer fluxes in k-space, and the 4/5 and 4/3 laws for third-order structure functions. Unexpectedly, the geometry of the pseudo-enstrophy $\Omega_w(\boldsymbol{x},t) = (\nabla \times \boldsymbol{w})^2$ is sheetlike, described similarly as $\Omega_\theta(\boldsymbol{x},t) = (\nabla\theta)^2$ for passive scalar, and unlike the tubelike structure of velocity. Since the equations for $\boldsymbol{u}$ and $\boldsymbol{w}$ both incorporate the (pseudo) pressure term to ensure incompressibility, we argue that the tubelike structure is not caused by pressure, but rather by the local nonlinear dynamics, while the sheetlike structure is considered a result of the linear convective effect (recall the sheetlike structure of the current sheet in the MHD turbulence).

The properties of passive vectors, such as the transfer efficiency, strength of the bottleneck effect, ratio of nonlocal to local transport, and scaling exponents of the increments and flux moments, are intermediate between those of velocity and passive scalars. At small scales, the properties of passive vectors are similar to those of passive scalars comparing to those of velocity. We interpret this as follows: firstly, the term $\omega_j \partial_j u_i$ of Eq.(2.50) is nonlinear in the velocity gradients and causes self-stretching of the vorticity, yielding a vortex tube. On the other

hand, $\zeta_j \partial_j u_i + \epsilon_{ijk} \partial_j w_l \partial_k u_l$ of Eq. (2.54) is bilinear and the alignment between $\boldsymbol{\zeta}$ and the eigenvector of the rate of strain tensor S^u_{ij} is disturbed by the second term. Then no tubelike structure is generated; instead, a sheetlike structure is formed. Secondly, the pressure p and pseudopressure q are determined through an integral weighted by the Poisson kernel. The differences between p and q arise from the small-scale structures of the source term of the Poisson equation. At large scales of p and q, the differences of the source terms at small scales are burried due to spatial integration, causing the amplitudes of p and q to appear nearly uniform in space. This means that the difference between ∇p and ∇q is very small, i.e., they act similarly. However, at small scales, ∇p and ∇q behave differently because of the difference in the source terms, leading to formation of thin sheetlike structure for the passive fields. The scaling exponents of the velocity are anomalous and universal, while those of the passive vector and scalar are anomalous, non-universal for high orders, and smaller than the velocity, and the strength of the intermittency is intermediate between that for velocity and passive scalars.

From the above observation and arguments we conclude that as for the low order statistics the fluctuations of the turbulent velocity and the passive fields convected by it are similar, but differ for the high order statistics. The nonlinearity of the Navier-Stokes equation leads anomalous but universal scaling exponents and the linearity of the quations of the passive fields bears nonuniversal scaling exponents and stronger intermittency than the velocity.

Acknowledgements

I am grateful for my supervisor Prof. Gotoh, who has paid large amount of energy for taking care of me, because that I had been completely an amateur on the fluid physics when I started my study at graduated school. The helpful advices and directional jobs from Prof. Miura are indispensable for all the processes of this study.

I also thank Prof. T. Watatane, Dr. Saito, Dr. Wang and Dr. Yasuda for their helpful discussions and comments. The National Institute for Fusion Science of Japan (NIFS16KNSS076, NIFS18KNSS105) is greatly acknowledged for providing computational resources. Also Networking, Large-scale Data Analyzing and Information Systems (JHPCN) (jh180009, jh190018) and High Performance Computing (HPC2018) at Nagoya University are acknowledged.

Appendix A

Derivation of von Kárman-Howarth Equations

The von Karman Howarth equation is said as that the unique analytical statement on turbulence. The original version was derived for the longitudinal velocity correlation in NS turbulence by T. von Kármán and L. Howarth at 1938. Based on it, Kolmogorov's 4/5 law[2] and Yaglom's 4/3 law[7] were given, which are related with most of work on statistical theory on turbulence. The idea was extended to more generic cases, especially MHD,[72] Hall MHD[73] and turbulent dynamo problem in sub-viscous range.[74]

A.1 Statistics in Homogeneous Isotropic Fields

Before deriving the von Kárman-Howarth equation, we brieftly describe the statistical expressions for several correlation functions for the statistically homogeneous isotropic random fields.

From the symmetry argument, first, second and third order isotropic tensor F_i, F_{ij} and F_{ijk} are of the form of:

$$F_i(r) = Ar_i \tag{A.1}$$

$$F_{ij}(r) = Ar_ir_j + B\delta_{ij} \tag{A.2}$$

$$F_{ijk}(r) = Ar_ir_jr_k + B\delta_{jk}r_i + C\delta_{ki}r_j + D\delta_{ij}r_k \tag{A.3}$$

where A, B, C and D are scalar functions of r only.

For the later argument, we consider first the $\langle u_k \varphi' \rangle$ where $\varphi' = \varphi(\boldsymbol{x}')$ is a scalar funtion. Taking the divergence, we hace

$$\partial_{r_k} \langle u_k \varphi' \rangle = r^{1-\mathcal{D}} \partial_r (r^{\mathcal{D}-1} K), \tag{A.4}$$

Where $\mathcal{D}$ is the spatial dimensionality. From the continuous equation, $\partial_{r_k} \langle u_k \varphi' \rangle = \partial_{x_k} \langle u_k \varphi' \rangle = 0$, so that

$$\begin{aligned} \partial_r (r^{\mathcal{D}-1} K) &= 0, \\ K &= C r^{1-\mathcal{D}}, \end{aligned}$$

but the finiteness of $k(r)$ at $r = 0$ requires $C = 0$, then

$$\langle u_k \varphi' \rangle = 0. \tag{A.5}$$

We define the two point velocity correlation function as

$$Q_{ij}(\mathbf{r}) = \langle u_i(\mathbf{x}) u_j(\mathbf{x}+\mathbf{r}) \rangle = \langle u_i u_j' \rangle = Q_{ji}(-\boldsymbol{r}), \tag{A.6}$$

where $u_j' = u_j(\boldsymbol{x}') = u_j(\boldsymbol{x}+\boldsymbol{r})$, and $Q_{ij}(\boldsymbol{r})$ can be written by the isotropy as

$$Q_{ij}(\mathbf{r}) = r_i r_j F(r) + \delta_{ij} G(r), \tag{A.7}$$

where $F(r)$ and $G(r)$ are scalar function of r alone. We define the operators

$$P_{ij}(\mathbf{r}) = \delta_{ij} - \frac{r_i r_j}{r^2}, \qquad \Pi_{ij}(\mathbf{r}) = \frac{r_i r_j}{r^2}, \tag{A.8}$$

then the longitudinal and transverse correlation functions are defined as

$$u_0^2 f(r) \equiv \langle u_L u_L' \rangle = \Pi_{ij}(\mathbf{r}) Q_{ij}(\mathbf{r}) = r^2 F + G, \tag{A.9}$$

$$u_0^2 g(r) \equiv \langle u_T u_T' \rangle = \frac{1}{\mathcal{D}-1} \mathrm{P}_{ij}(\mathbf{r}) Q_{ij}(\mathbf{r}) = G, \tag{A.10}$$

where u_L and u_T are components parallel and perpendicular to $\boldsymbol{r}$, respectively, and

$$Q_{ij}(\mathbf{r}) = u_0^2 \{ \mathrm{P}_{ij}(\boldsymbol{r}) g(r) + \Pi_{ij}(\boldsymbol{r}) f(r) \}, \qquad u_0^2 = \frac{1}{\mathcal{D}} |\boldsymbol{u}|^2. \tag{A.11}$$

The incompressibility implies

$$\partial_{r_i} Q_{ij} = \partial_i \langle u_i(\mathbf{x}) u_j(\mathbf{x}') \rangle = \left\langle (\partial_i u_i) u_j' \right\rangle = 0, \tag{A.12}$$

and applying to Eq. (A.11) yields

$$\frac{2}{r}g = \left(\frac{2}{r} + \frac{d}{dr}\right) f \tag{A.13}$$

Finally, we arrive at

$$Q_{ij}(\mathbf{r}) = u_0^2 \left[f(r)\delta_{ij} + \frac{r}{2}\frac{df}{dr} P_{ij}(\boldsymbol{r}) \right]. \tag{A.14}$$

Similarly, we consider the third order correlation as

$$Q_{ijk}(\mathbf{r}) = \langle u_i u_j u_k' \rangle. \tag{A.15}$$

From the incompressibility condition,

$$\partial_k Q_{ijk}(\mathbf{r}) = 0. \tag{A.16}$$

Substituting into Eq. (A.3), we obtain

$$r\partial_r A + 5A + r^{-1}\partial_r B + r^{-1}\partial_r C = 0, \tag{A.17}$$

$$r\partial_r D + 3D + B + C = 0. \tag{A.18}$$

Since

$$Q_{ijk}(\mathbf{r}) = Q_{jik}(\mathbf{r}), \tag{A.19}$$

we have

$$B = C. \tag{A.20}$$

From Eq. (A.15), we have $\partial_k Q_{iik}(\boldsymbol{r}) = 0$, meaning that $Q_{iik}(\boldsymbol{r}) = 0$ because of the regularity at $r = 0$, so that

$$Ar^2 + 2B + 3D = 0 \tag{A.21}$$

From the above equations A, B, C are expressed in terms of D alone as

$$A = \frac{\partial_r}{r} D, \tag{A.22}$$

$$B = C = -\frac{1}{2}(r\partial_r + 3)D. \tag{A.23}$$

The longitudinal third order correlation function $h(r)$ is defined by

$$u_0^3 h(r) = \langle u_L u_L u'_L \rangle, \tag{A.24}$$

and we arrive at

$$u_0^3 h(r) = -2rD, \tag{A.25}$$

$$Q_{ijk}(\mathbf{r}) = u_0^3 \left\{ \frac{h - r\partial_r h}{2} \frac{r_i r_j r_k}{r^3} + \frac{2h + r\partial_r h}{4} \left(\frac{r_i}{r}\delta_{jk} + \frac{r_i}{r}\delta_{ik} \right) - \frac{h}{2}\frac{r_k}{r}\delta_{ij} \right\}. \tag{A.26}$$

A.2 von Kárman-Howarth Equations and Kolmogorov's 4/5 Law

Incompressible Navier-Stokes equation and continuous equation are given as

$$\partial_t u_i + u_l \partial_l u_i = -\partial_i p + \nu \partial_{ll}^2 u_i, \tag{A.27}$$

$$\partial_i u_i = 0. \tag{A.28}$$

By writing $\partial'_i = \partial_{i'}$, $u'_i = u_i(\mathbf{x}')$, we obtain the evolution of $u_j(\mathbf{x}')$ as,

$$\partial_t u'_j + u'_l \partial'_l u'_i = -\partial'_i p' + \nu \partial'^2_{ll} u'_i. \tag{A.29}$$

Multiplying Eq. (A.27) by u'_j and Eq. (A.29) by u_i, and adding them yield

$$\begin{aligned} u'_j \partial_t u_i + u_i \partial_t u'_j = &- u'_j u_l \partial_l u_i - u_i u'_l \partial'_l u'_i - \langle \partial_i p u'_i \rangle - \langle u_i \partial'_j p' \rangle \\ &+ u'_j \nu \partial_{ll}^2 u_i + u_i \nu \partial'^2_{ll} u'_i, \end{aligned} \tag{A.30}$$

By noting that $u'_j u_l \partial_l u_i = u_l \partial_l (u_i u'_j) = \partial_l (u_l u_i u'_j)$ and taking the ensemble averaging, we obtain

$$\partial_t \langle u_i u'_j \rangle = -\partial_l \langle u_l u_i u'_j \rangle - \partial'_l \langle u'_l u_i u'_j \rangle + \nu \partial_{ll}^2 \langle u_i u'_j \rangle + \nu \partial'^2_{ll} \langle u_i u'_j \rangle \tag{A.31}$$

The pressure term in Eq. (A.31) vanishes by Eq. (A.5), then Eq. (A.31) is written as as

$$\partial_t Q_{ij} = -\partial_l Q_{lij} + \partial'_l Q_{lji} + \nu \partial_{ll}^2 Q_{ij} + \nu \partial'^2_{ll} Q_{ij}, \tag{A.32}$$

Noting that the derivative on $\frac{\partial}{\partial x_i}$ could be rewritten as $\frac{\partial}{\partial r_i}$ form, as

$$\partial_{l'} Q_{lji} = \partial_{r_l} Q_{lji}, \tag{A.33}$$

$$\partial_l Q_{lij} = -\partial_{r_l} Q_{lij}, \tag{A.34}$$

and taking the trace, namely $i = j$, we have

$$\partial_t Q_{ii} = 2\partial_l Q_{lii} + 2\nu \partial_{ll}^2 Q_{ii}. \tag{A.35}$$

Substitution of Eq. (A.14) and Eq. (A.26) gives

$$\begin{aligned} \partial_t u_0^2 [3f + r\partial_r f] =& 2\partial_{r_l} u_0^3 X_1 + 2\nu X_2, \\ X_1 =& \frac{1}{2}\frac{r_l}{r}(4h + rh'), \\ X_2 =& (3 + r\partial_r)(\frac{4\partial_r}{r} + \partial_{rr}^2) f. \end{aligned} \tag{A.36}$$

Using operator $\mathcal{L}A = r^{-2}\partial_r(r^3 A) = 3A + rA'$, the above Eq. (A.36) is written as

$$\mathcal{L}\left\{\partial_t u_0^2 f - \left(\partial_r + \frac{4\partial_r}{r}\right) u_0^3 h - 2\nu \left(\frac{4}{r} + \partial_{rr}^2\right) u_0^2 f\right\} = 0,$$

$$\partial_t u_0^2 f - \left(\partial_r + \frac{4}{r}\right) u_0^3 h - 2\nu \left(\frac{4\partial_r}{r} + \partial_{rr}^2\right) u_0^2 f = C r^{-3}.$$

Regularity at $r = 0$ requires $C = 0$, then the above equation becomes

$$\partial_t u_0^2 f = \left(\partial_r + \frac{4}{r}\right) u_0^3 h + 2\nu \left(\frac{4\partial_r}{r} + \partial_{rr}^2\right) u_0^2 f. \tag{A.37}$$

Importing structure functions as $S_n(r) = \langle (u_L' - u_L)^n \rangle = \langle (\delta u_L)^n \rangle$, applying homogeneity and isotropy, we have

$$S_2 = Q_{L'L'} - 2Q_{L'L} + Q_{LL} = 2u_0^2(1 - f), \tag{A.38}$$

$$S_3 = Q_{L'L'L'} - 3Q_{L'L'L} + 3Q_{LLL'} - Q_{LLL} = 6Q_{LLL'} = 6u_0^3 h, \tag{A.39}$$

where $Q_{LL'} \equiv \langle u_L(\boldsymbol{x}) u_L(\boldsymbol{x}') \rangle$ and $Q_{LLL'} \langle \equiv u_L(\boldsymbol{x}) u_L(\boldsymbol{x}) u_L(\boldsymbol{x}') \rangle$, respectively. Substituting Eq. (A.38) and Eq. (A.39) into Eq. (A.37), leads

$$\partial_t u_0^2 - \frac{1}{2}\partial_t S_2(r,t) = \left(\partial_r + \frac{4}{r}\right)\frac{S_3}{6} - \frac{\nu}{r^4}\frac{\partial}{\partial r}\left(r^4 \frac{\partial S_2}{\partial r}\right). \tag{A.40}$$

In the inertial range the viscous term can be dropped and in statistically steady state the term $\partial_t S_2 = 0$

$$\partial_t u_0^2 = \left(\partial_r + \frac{4}{r}\right)\frac{S_3}{6}.$$

By the definition of the mean kinetic energy dissipation rate per mass $\bar{\epsilon} = -\partial_t\langle|\mathbf{u}|^2/2\rangle = -\frac{3}{2}\partial_t u_0^2$, it yields

$$\begin{aligned} -4\bar{\epsilon} =& r^{-4}\partial_r(r^4 S_3), \\ S_3 =& -\frac{4}{5}r\bar{\epsilon} + Cr^{-4}, \end{aligned}$$

The regularity at $r = 0$ requires,

$$\langle(\delta u_L)^3\rangle = -\frac{4}{5}\bar{\epsilon}r, \tag{A.41}$$

which is the Kolmogorov's 4/5 law.

A.3 vKH Equations for Passive Fields and 4/3 Law

Applying the similar procedure to the velocity to the equation for the passive scalar:

$$\partial_t\theta + \mathbf{u}\cdot\nabla\theta = \kappa\nabla^2\theta, \tag{A.42}$$

it leads to,

$$\partial_t Q^\theta = 2\partial_i Q_i^\theta + 2\kappa\partial_r^2 Q^\theta, \tag{A.43}$$

where the correlation functions f_θ and h_θ are defined as,

$$Q^\theta(\mathbf{r}) = \langle\theta\theta'\rangle = \theta_0^2 f_\theta(r), \tag{A.44}$$

$$Q_i^\theta(\mathbf{r}) = \langle u_i\theta\theta'\rangle = u_0\theta_0^2 r_i h^\theta(r). \tag{A.45}$$

Substituting Eqs. (A.44) and (A.45) into Eq. (A.43), we obtain the von Kárman-Howarth equation from the passive scalar as

$$\partial_t\theta_0^2 f_\theta = \left(\frac{4}{r} + 2\partial_r\right)u_0\theta_0^2 h_\theta + 2\kappa(\frac{2}{r} + \partial_{rr}^2)\theta_0^2 f_\theta. \tag{A.46}$$

The moments of the increments are related to the correlation functions as

$$S_2^\theta = \langle (\delta\theta)^2 \rangle = 2\theta_0^2(1 - f_\theta), \tag{A.47}$$

$$\Pi^\theta = \langle (\delta u_L)(\delta\theta)^2 \rangle = 4u_0\theta_0^2 h_\theta, \tag{A.48}$$

where $\langle \theta^2 u_L' \rangle = 0$ and $\langle \theta^2 u_L \rangle = \langle \theta'^2 u_L' \rangle$ are used. Substituting Eq. (A.47) and Eq. (A.48) into Eq. (A.46), we obtain that

$$-2\bar{\epsilon}_\theta - \frac{1}{2}\partial_t S_2^\theta = \frac{1}{2}(\frac{2}{r} + \partial_r)\Pi^\theta - \kappa(\frac{2}{r}\partial_r + \partial_{rr}^2)S_2^\theta, \tag{A.49}$$

since $\bar{\epsilon}_\theta = -\frac{d}{dt}\langle \theta^2/2 \rangle = -\frac{1}{2}\partial_t\theta_0^2$, at the statistically steady steady the second term of L.H.S vanishes, and the diffusive term is negligible in the inertial-convective range. Integrating the above equation and taking into regularity at $r = 0$, we obtain the Yaglom's 4/3 law,

$$\langle (\delta u_L)(\delta\theta)^2 \rangle = -\frac{4}{3}\bar{\epsilon}_\theta r. \tag{A.50}$$

An imcompressible passive vector is governed by

$$\partial_t w_i + u_j\partial_j w_i = -\partial_i q + \alpha\partial_{jj}^2 w_i, \qquad \partial_i w_i = 0. \tag{A.51}$$

The equation for the correlation function Q_{ij}^w is given by,

$$\partial_t Q_{ij}^w = -2\partial_k Q_{ijk}^w + 2\alpha\partial_{rr}^2 Q_{ij}^w, \tag{A.52}$$

Similarly as Before, we have the following expressions,

$$Q_{ij}^w = \langle w_i w_j \rangle = w_0^2 \left[\delta_{ij} f^w(r) + P_{ij}\frac{r}{2}\frac{df}{dr} \right], \tag{A.53}$$

$$Q_{ijk}^w = \langle u_i w_j w_k \rangle = u_0 w_0^2 \left\{ \frac{r_i r_j r_k}{r^3}\frac{h^w - r\frac{\partial h^w}{\partial r}}{2} + \frac{r_i\delta_{jk}}{r}q^w \right. \tag{A.54}$$

$$\left. + \left[\frac{r_j\delta_{ik}}{r}\left(h^w + r\frac{\partial h^w}{\partial r} - q^w \right) \right] - \frac{r_k}{r}\delta_{ij}\frac{h}{2} \right\}, \tag{A.55}$$

where the scalar functions $f^w(r)$, $h^w(r)$ and $q^w(r)$ are defined as

$$w_0^2 f^w(r) = \langle w_L(\boldsymbol{x}) w_L(\boldsymbol{x}') \rangle, \tag{A.56}$$

$$u_0 w_0^2 h^w(r) = \langle u_L(\boldsymbol{x}) w_L(\boldsymbol{x}) w_L(\boldsymbol{x}') \rangle, \tag{A.57}$$

$$u_0 w_0^2 q^w(r) = \langle u_L(\boldsymbol{x}) w_T(\boldsymbol{x}) w_T(\boldsymbol{x}') \rangle. \tag{A.58}$$

Substituting Eqs. (A.53) and (A.55) into Eq. (A.52), we obtain the von Kárman-Howarth equation for the passive vector,

$$\frac{\partial}{\partial t}f^w(r) = \frac{2}{r}u_0 w_0^2[h^w(r) + 2q^w(r)] + 2\alpha\left(\frac{\partial^2}{\partial r^2} + \frac{4}{r}\frac{\partial}{\partial r}\right)w_0^2 f^w(r). \tag{A.59}$$

Then defining the moments of increments similar to the passive scalar as

$$S_2^w(r) = \langle (w'_L - w_L)^2\rangle, \tag{A.60}$$

$$\Pi^w(r) = \langle (u'_L - u_L)(\boldsymbol{w}' - \boldsymbol{w})^2\rangle. \tag{A.61}$$

Performing same procedures and conditions from Eq. (A.46) to Eq. (A.50), we arrive the 4/3 law for the passive vector

$$-\frac{4}{3}\overline{\epsilon}_w r = \langle \delta u_L |\delta \boldsymbol{w}|^2\rangle. \tag{A.62}$$

In this context, it is worthwhile to consider the similar relation to the MHD turbulence. The MHD equation is usually used in studies of the electric conductive fluid, as

$$\left(\frac{\partial}{\partial t} + \boldsymbol{u}\cdot\nabla\right)\boldsymbol{u} = -\nabla p + (\nabla\times\boldsymbol{b})\times\boldsymbol{b} + \nu\nabla^2\boldsymbol{u}, \qquad \nabla\cdot\boldsymbol{u} = 0, \tag{A.63}$$

$$\frac{\partial}{\partial t}\boldsymbol{b} = \nabla\times(\boldsymbol{u}\times\boldsymbol{b}) + \lambda\nabla^2\boldsymbol{b}, \qquad \nabla\cdot\boldsymbol{w} = 0, \tag{A.64}$$

where $\boldsymbol{b}(\boldsymbol{x}, t)$ denotes for the normalized magnetic field, and λ for the normalized diffusive coefficient of magnetic field, respectively. The Elsässer varibles are defined as

$$\boldsymbol{z}^{\pm} = \boldsymbol{u} \pm \boldsymbol{b}, \tag{A.65}$$

then Eqs. (A.63) and (A.64) are simplified as

$$\left(\frac{\partial}{\partial t} + \boldsymbol{z}^{\mp}\cdot\nabla\right)\boldsymbol{z}^{\pm} = -\nabla p_b + \nu^+\nabla^2\boldsymbol{z}^{\pm} + \nu^-\nabla^2\boldsymbol{z}^{\mp}, \qquad \nabla\cdot\boldsymbol{z}^{\pm} = 0, \tag{A.66}$$

where $p_b = p + \frac{\boldsymbol{b}^2}{2}$, $\nu^+ = \frac{\nu+\lambda}{2}$ and $\nu^- = \frac{\nu-\lambda}{2}$. In the case both $Pr_m = \frac{\nu}{\lambda} = 1$, Eq. (A.66) is equivalent to Eq. (A.51), von Kárman-Howarth equation and 4/3 law for Elsässer varibles can be easily derived, replacing $\boldsymbol{w}$ with $\boldsymbol{z}^+$, $\boldsymbol{u}$ with $\boldsymbol{z}^-$ and q with p_b, or replacing $\boldsymbol{w}$ with $\boldsymbol{z}^-$, $\boldsymbol{u}$ with $\boldsymbol{z}^+$,

$$\frac{\partial}{\partial t}f^{z^{\pm}}(r) = \frac{2}{r}z_0^{\mp}(z_0^{\pm})^2[h^{\pm}(r) + 2q^{\pm}(r)] + 2\nu\left(\frac{\partial^2}{\partial r^2} + \frac{4}{r}\frac{\partial}{\partial r}\right)(z_0^{\pm})^2 f^{z^{\pm}}(r), \tag{A.67}$$

$$-\frac{4}{3}\overline{\epsilon}_z^{\pm} r = \langle \delta z_L^{\mp} |\delta \boldsymbol{z}^{\pm}|^2\rangle. \tag{A.68}$$

References

[1] O. Reynolds. An experimental investigation of the circumstances which determine whether the motion of water shall be direct or sinuous, and of the law of resistance in parallel channels. *Royal Soc. of Lond.*, 174, 1883. 1

[2] A. N. Kolmogorov. The local structure of turbulence in incompressible viscous fluid for very large reynolds' numbers. *Dokl. Akad. Nauk SSSR*, 32:16, 1941. 1, 5, 19, 73

[3] Y. Tsuji. High-reynolds-number experiments: the challenge of understanding universality in turbulence. *Fluid Dyn. Res.*, 41:17, 2009. 3

[4] T. Gotoh and P. K. Yeung. *Passive scalar transport in turbulence*, chapter 10. Cambridge University Press, 2013. 5

[5] T. Ishihara, T. Gotoh, and Y. Kaneda. Study of high reynolds number isotropic turbulence by direct numerical simulation. *Annu. Rev. Fluid Mech.*, 41, 2009. 5, 37, 38

[6] A. M. Obukhov. The structure of the temperature field in a turbulent flow. *Izv. Akad. Nauk SSSR*, 69:743, 1949. 6

[7] A. M. Yaglom. Structure of temperature field in turbulent flow. *Dokl. Akad. Nauk SSSR*, 69:743, 1949. 6, 18, 73

[8] S. Corrsin. On the spectrum of isotropic temperature fluctuations in isotropic turbulence. *J. Appl. Phys.*, 22:469, 1951. 6

[9] G. K. Batchelor. Small-scale variantion of convected quantities like temperature in turbulent fluid. part 1: General discussion and the case of small conductivity. *J. Fluid Mech.*, 5:113, 1959. 6

[10] G. K. Batchelor, I. K. Howells, and A. A. Towsend. Small-scale variantion of convected quantities like temperature in turbulent fluid. part 2: The case of large conductivity. *J. Fluid Mech.*, 5:134, 1959. 6

[11] R. H. Kraichnan. Small scale structure of a scalar field convected by turbulence. *Phys. of Fluid*, 11:945, 1968. 6

[12] R. A. Antonia, E. J. Hopfinger, Y. Gagne, and F. Anselmet. Temperature structure functions in turbulent shear flows. *Phys. Rev. A*, 30, 1998. 6

[13] A. Celani, A. Lanotte, A. Mazzino, and M. Vergassola. Universality and saturation of intermittency in passive scalar turbulence. *Phys. Rev. Lett.*, 84:2385, 2000. 6

[14] F. Moisy, H. Willaime, J. S. Andersen, and P. Tabeling. Passive scalar intermittency in low temperature helium flows. *Phys. Rev. Lett.*, 86, 2001. 6

[15] T. Watanabe and T. Gotoh. Statistics of a passive scalar in homogeneous turbulence. *New J. Phys.*, 6:40, 2004. 6, 26, 37, 38, 43, 50, 58, 60

[16] T. Watanabe and T. Gotoh. Intermittency in passive scalar turbulence under the uniform mean scalar gradient. *Phys. of Fluid*, 18(058105), 2006. 6

[17] E. W. Saw, P. Debue, D. Kuzzay, F. Daviaud, and B. Dubrulle. On the universality of anomalous scaling exponents of structure functions in turbulent flows. *J. Fluid Mech.*, 837:657, 2018. 6

[18] H. Stapoutzis, B. L. Sawford, J. C. R. Hunt, and R. E. Britter. Structure of the temperature field downwind of a line source in grid turbulence. *J. Fluid Mech.*, 165:401, 1986. 6

[19] H. Jiménez, A. A. Wray, P. G. Saffman, and R. S. Rogallo. The structure of intense vorticity in isotropic turbulence. *J. Fluid Mech.*, 255:65, 1993. 6, 32

[20] T. Gotoh and T. Watanabe. Scalar flux in a uniform mean scalar gradient in homogeneous isotropic turbulence. *Physica D*, 241:141, 2012. 6, 43

[21] R. H. Kraichnan. Anomalous scaling of a randomly advected passive scalar. *Phys. Rev. Lett.*, 72:1016, 1994. 6

[22] K. Gawedzki and A. Kupiainen. Anomalous scaling of passive scalar. *Phys. Rev. Lett.*, 75:3834, 1995. 6

[23] M. Vergassola. Anomalous scaling for passive advected magnetic fields in low temperature helium flows. *Phys. Rev. E*, 53:3012, 1996. 6

[24] A. Celani, A. Lanotte, A. Mazzino, and M. Vergassola. Fronts in passive scalar turbulence. *Phys. of FLuid*, 13:1768, 2001. 6, 43, 50

[25] K. Gawedzki and M. Vergassola. Phase transition in the passive scalar advection. *Physica D*, 138:63, 2000. 6

[26] G. Falkovich, K. Gawedzki, and M. Vergassola. Particles and fields in fluid turbulence. *Rev. Mod. Phys.*, 73:913, 2001. 6

[27] T. Gotoh and T. Watanabe. Power and non-power laws of passive scalar moments convected by isotropic turbulence. *Phys. Rev. Lett.*, 115(114502), 2015. 6, 60

[28] K. Yoshida and Y. Kaneda. Anomalous scaling of anisotropy of second-oreder moments in a model of a randomly advected solenoidal vector field. *Phys. Rev. E*, 63(016308), 2000. 7

[29] L. Ts. Adzhemyan, N. V. Antonov, A. Mazzino, P. M. Muratore-Ginanneschi, and A. V. Runov. Pressure and intermittency in passive vector turbulence. *Europhys. Lett.*, 55, 2001. 7

[30] K. Ohkitani. Numerical study of comparison of vorticity and passive vector in turbulence and inviscid flows. *Phys. Rev. E*, 65(046304), 2002. 7

[31] R. Benzi, L. Biferale, and F. Toschi. Universality in passively advected hydrodynamic fields: the case of a passive vector with pressure. *Eur. phys. J. B*, 24, 2001. 8, 60

[32] E. S. C. Ching, Y. Cohen, T. Gilbert, and I. Procaccia. Active and passive fields in turbulent transport: the role of statistically preserve structures. *Phys. Rev. E*, 67(016304), 2003. 8

[33] N. V. Antonov, M. Hnatich, J. Honkonen, and M. jurčiĭn. Turbulence with pressure: Anomalous scaling of a passive vector field. *Phys. Rev. E*, 68(046306), 2003. 8, 60

[34] N. V. Antonov and N. M. Guliskiy. Anisotropic turbulent advection of a passive vector field: Effect of the finite correlation time. *EPJ Web Conf*, 108(02008), 2016. 8

[35] H Arponen. Steady-state existence of passive vector field under the krainchnan model. *Phys. Rev. E*, 81(036325), 2010. 8

[36] L. Howarth T. von Kármán. On the statistical theory of isotropic turbulence. *Proc. R. Soc. London Ser. A*, 164:192, 1938. 17

[37] L. D Landau. and E. M. Lifshitz. *Fluid Mechanics 2nd Edition.* Pergamon, 1987. 21

[38] A. N. Kolmogorov. A refinement of previous hypothese concerning the loacal structure of turbulence in a viscous incompressible fluid at high reynolds number. *J. Fluid Mech*, 12:82, 1962. 21, 53

[39] U. Frisch. *Turbulence: The legacy of A. N. Kolmogorov.* Cambridge University Press, 1995. 21

[40] T. Gotoh. *the basis of turbulence theory(in Japanese).* Asakura Publishing, 1998. 21

[41] Z-S. She and E. Lévêque. Universal scaling laws in fully developed turbulence. *Phys. Rev. Lett.*, 72:336, 1994. 21

[42] T. Watanabe and T. Gotoh. Inertial-range intermittency and accuracy of direct numerical simulation for turbulence and passive scalar turbulence. *J. Fluid Mech.*, 590:117, 2007. 26, 27, 59

[43] D. A. Donzis and P. K. Yeung. Resolution effects and scaling in numerical simulations of passive scalar mixing in turbulence. *Physica D*, 239:1278, 2010. 26

[44] T. Gotoh, S. Hanataka, and H. Miura. Spectral compact difference hybrid computation of passive scalar in isotropic turbulence. *J. Compu. Phys.*, 231:7398, 2012. 26, 27

[45] D. A. Donzis and K. R. Sreenivasan. The bottleneck effect and kolmogorov constant in isotropic turbulence. *J. Fluid Mech.*, 657:171, 2010. 27, 36, 37, 43

[46] R. Prasad and K. R. Sreenivasan. Quantitative three dimensional imaging and the structure of passive scalar fields in fully turbulent flows. *J. Fluid Mech.*, 216:1, 1990. 32

[47] K. A. Buch and W. J. A. Dahm. Experimental study of the fine-scale structure of conserved sclar mixing in turbulent shear flows. part 1: $sc \gg 1$. *J. Fluid Mech.*, 317:21, 1996. 32

[48] T. Gotoh, T. Watanabe, and H. Miura. Spectrum of passive scalar at very high schmit number in turbulence. *Plas. Fusion Res.*, 9(3401019), 2014. 32

[49] T. Gotoh, D. Fukuyama, and T. Nakano. Velocity field statistics in homogeneous steady turbulence obtained using a high-resolution direct numerical simulation. *Phys. Fluids*, 14:1065, 2002. 37, 50, 52, 58, 59

[50] Y. Kaneda, T. Ishihara, M. Yokokawa, K. Itakura, and A. Uno. Energy dissipation rate and energy spectrum in high resolution direct simulation of turbulence in a periodic box. *Phys. Fluids*, 15:L21, 2003. 37

[51] T. Gotoh and D. Fukuyama. Pressure spectrum in homogeneous turbulence. *Phys. Rev. Lett.*, 86:3775, 2001. 40

[52] Y. Tsuji and Y. Kaneda. Anisotropic pressure correlation spectra in turbulent shear flow. *J. Fluid Mech.*, 694:50, 2012. 40

[53] K. R. Sreenivasan, R. A. Antonia, and D. Britz. Local isotropy and large structures in a heated turbulent jet. *J. Fluid Mech.*, 94:745, 1979. 43

[54] K. R. Sreenivasan. On local isotropy of passive scalar in turbulent shear flows. *Proc. R. Soc. London A*, 434:165, 1991. 43

[55] M. Holzer and E. D. Siggia. Turbulent mixing of a passive scalar. *Phys. Fluids*, 6:1820, 1994. 43

[56] G. Folkovich. Bottleneck phenomenon in developed turbulence. *Phys. Fluids*, 6:1411, 1994. 43

[57] Y. Kaneda. Renormalized expansions in the theory of turbulence with the use of the lagrangian position function. *J. Fluid Mech.*, 107:131, 1981. 44

[58] Y. Kaneda. Inertial range structure of turbulent velocity and scalar fields in a lagrangian renormalized approximation. *Phys. Fluids*, 29:701, 1986. 44

[59] T. Gotoh. Passive scalar diffusion in two dimensional turbulence in the lagrangian renormalized approximation. *J. Phys. Soc. Jpn.*, 58:2365, 1989. 44

[60] T. Gotoh and T. Watanabe. Statistics of transfer fluxes of the kinetic energy and scalar variance. *J. Turbul.*, 6:33, 2005. 44

[61] P. D. Mininni, A. Alexakis, and A. Pouquet. Nonlocal interactions in hydrodynamics turbulence at high reynolds numbers: The slow emergence of scaling laws. *Phys. Rev. E*, 77(036306), 2008. 47

[62] J. A. Domaradzki and Daniele Carati. An analysis of the energy transfer and the locality of nonlinear interactions in turbulence. *Phys. of Fluids*, 19(085112), 2007. 47

[63] T. Gotoh, T. Watanabe, Y. shiga, T. Nakano, and E.suzuki. Statistical properties of four-dimensional turbulence. *Phys. Rev. E*, 75(016310), 2007. 50

[64] Jayesh and Z.Warhaft. Probability distribution of a passive scalar in grid-generated turbulence. *Phys. Rev. Lett.*, 67:3503, 1991. 50

[65] Jayesh and Z.Warhaft. Probability distribution, conditional dissipation, and tranport of passive temperature fluctuations in grid-generated turbulence. *Phys. Fluids A*, 4:2292, 1992. 50

[66] E. S. C. Ching and Y. Tu. Passive scalar fluctuations with and without a mean gradient: A numerical study. *Phys. Rev. E*, 49:1278, 1994. 50

[67] A. Bourlioux and A. J. Majda. Elementary models with probability distribution function intermittency for passive scalars with a mean gradient. *Phys. Fluids*, 14:881, 2002. 50

[68] N. Cao, S. Chen, and G. D. Doolen. Statistics and structures of pressure in isotropic turbulence. *Phys. Fluids*, 11:2235, 1999. 51

[69] T. Gotoh and R. S. Rogallo. Intermittency and scaling of pressure at small scales in forced isotropic turbulence. *J. Fluid Mech.*, 396:285, 1999. 51, 52

[70] T. Gotoh and R. H. Kraichnan. Turbulence and tsallis statistics. *Physica D*, 193:231, 2004. 52

[71] D. Buraia, A. Pumir, E. Bordenschatz, and P. K. Yeung. Extreme velocity gradients in turbulent flows. *New J. Phys.*, 21(043004), 2019. 56

[72] H. Politano and A. Pouquet. von kármán?howarth equation for magnetohydrodynamics and its consequences on third-order longitudinal structure and correlation functions. *Phys. Rev. E*, 57(R21), 1998. 73

[73] S. Galtier. von kármán?howarth equations for hall magnetohydrodynamic flows. *Phys. Rev. E*, 77(015302), 2008. 73

[74] T. A. Yousef, F. Rinco, and A. A. Schekochihin. Exact scaling laws and the local structure of isotropic magnetohydrodynamic turbulence. *J. Fluid Mech.*, 575:110, 2007. 73